Acta Pharmaceutica Sinica B 2025;15(2):892–908

Chinese Pharmaceutical Association
Institute of Materia Medica, Chinese Academy of Medical Sciences

Acta Pharmaceutica Sinica B

www.elsevier.com/locate/apsb
www.sciencedirect.com

ORIGINAL ARTICLE

Intestinal stearoyl-coenzyme A desaturase-inhibition improves obesity-associated metabolic disorders

Yangliu Xia[a,†], Yang Zhang[c,†], Zhipeng Zhang[d,†], Nana Yan[a,b], Vorthon Sawaswong[a], Lulu Sun[e], Wanwan Guo[e], Ping Wang[a], Kristopher W. Krausz[a], Oksana Gavrilova[f], James M. Ntambi[g], Haiping Hao[b,*], Tingting Yan[a,b,*], Frank J. Gonzalez[a,*]

[a]*Cancer Innovation Laboratory, Center for Cancer Research, National Cancer Institute, National Institutes of Health, Bethesda, MD 20892, USA*
[b]*State Key Laboratory of Natural Medicines, Laboratory of Metabolic Regulation and Drug Target Discovery, China Pharmaceutical University, Nanjing 210009, China*
[c]*Section on Human Iron Metabolism, Eunice Kennedy Shriver National Institute of Child Health and Human Development, National Institutes of Health, Bethesda, MD 20892, USA*
[d]*Department of General Surgery, Cancer Center, Third Hospital, Peking University, Beijing 100191, China*
[e]*State Key Laboratory of Female Fertility Promotion, Department of Endocrinology and Metabolism, Third Hospital, Peking University, Beijing 100191, China*
[f]*Mouse Metabolism Core Laboratory, National Institute of Diabetes and Digestive and Kidney Diseases, National Institutes of Health, Bethesda, MD 20892, USA*
[g]*Department of Biochemistry, University of Wisconsin–Madison, Madison, WI 53706, USA*

Received 25 July 2024; received in revised form 21 October 2024; accepted 20 November 2024

KEY WORDS

Obesity;
SCD1;
MT1;
Intestinal epithelium;
High-fat diet;

Abstract Stearoyl-coenzyme A desaturase 1 (SCD1) catalyzes the rate-limiting step of *de novo* lipogenesis and modulates lipid homeostasis. Although numerous SCD1 inhibitors were tested for treating metabolic disorders both in preclinical and clinic studies, the tissue-specific roles of SCD1 in modulating obesity-associated metabolic disorders and determining the pharmacological effect of chemical SCD1 inhibition remain unclear. Here a novel role for intestinal SCD1 in obesity-associated metabolic disorders was uncovered. Intestinal SCD1 was found to be induced during obesity progression both in humans and

*Corresponding authors.
E-mail addresses: haipinghao@cpu.edu.cn (Haiping Hao), tingting.yan@cpu.edu.cn (Tingting Yan), gonzalef@mail.nih.gov (Frank J. Gonzalez).
[†]These authors made equal contributions to this work.
Peer review under the responsibility of Chinese Pharmaceutical Association and Institute of Materia Medica, Chinese Academy of Medical Sciences.

https://doi.org/10.1016/j.apsb.2024.11.022

Oxidative stress;
Steatosis;
Metabolic disorders

mice. Intestine-specific, but not liver-specific, SCD1 deficiency reduced obesity and hepatic steatosis. A939572, an SCD1-specific inhibitor, ameliorated obesity and hepatic steatosis dependent on intestinal, but not hepatic, SCD1. Mechanistically, intestinal SCD1 deficiency impeded obesity-induced oxidative stress through its novel function of inducing metallothionein 1 in intestinal epithelial cells. These results suggest that intestinal SCD1 could be a viable target that underlies the pharmacological effect of chemical SCD1 inhibition in the treatment of obesity-associated metabolic disorders.

1. Introduction

Obesity and the associated metabolic disorders are globally widespread chronic diseases that impair human health and increase economic burden[1,2]. The accumulation of excessive amounts of body fat drives multiple metabolic abnormalities and diseases, including insulin resistance, diabetes, cardiovascular disease, metabolic dysfunction-associated steatotic liver disease, and cancer[3]. Numerous medications were developed for obesity treatment by exploiting different mechanisms, among which the discovery and development of glucagon-like peptide 1 receptor (GLP-1R) agonist-based drugs that have been considered a transformative breakthrough in the field, and are now recognized promising medications for the treatment of obesity[4-6]. Despite the widespread use of GLP-1R agonist-based drugs, an increased risk for gastrointestinal side effects is of a major concern for the safety profile of GLP-1R agonists[7,8]. Thus, developing novel pharmacotherapies with suitable tolerability and safety for the treatment of obesity remains an ongoing challenge.

Obesity usually occurs accompanied with systemic oxidative stress, including elevated levels of reactive oxygen species (ROS) and deteriorated capability of antioxidant protection[9,10]. Oxidative stress is usually an expected result of obesity in humans or long-term chronic high-fat diet (HFD) feeding in mice[11,12]. Chronic HFD feeding-induced oxidative stress is also thought to causally contribute to weight gain and facilitate the development of insulin resistance since elevated oxidative stress can cause an increase in preadipocyte proliferation, adipocyte differentiation and the size of mature adipocytes, and suppress insulin signaling through phosphorylation of insulin receptor substrate[13]. Pharmacologically, *N*-acetylcysteine (NAC), an antioxidant listed as an essential drug by the World Health Organization, has shown therapeutic potential in treating obesity-associated complications by decreasing the intracellular antioxidant levels of adipocytes, leading to reduced inflammation and oxidative damage[14]. However, until now, the role of endogenous signaling transduction in modulating obesity-associated oxidative stress is still largely unknown.

Stearoyl-coenzyme A desaturase 1 (SCD1) is a key rate-limiting enzyme involved in lipid metabolism[15], with mouse SCD1 being homologous to human SCD[16]. SCD1 catalyzes the formation of a *cis* double bond between carbons 9 and 10 of saturated fatty acids, resulting in the formation of the respective Δ9 unsaturated monounsaturated fatty acid (MUFA) counterparts, primarily oleic acid (18:1) and palmitoleic acid (16:1), which are two key substrates for important lipids such as phospholipids, triglycerides, cholesteryl esters, and wax esters[17,18]. Global SCD1 deficient mice ($Scd1^{-/-}$) are resistant to HFD-induced obesity, accompanied by increased energy expenditure, with the phenotype partially recapitulated in skin-specific *Scd1*-null mice[19,20]. Liver-specific *Scd1*-null mice were reported to be protected from high-carbohydrate, but not high-fat, diet-induced adiposity and hepatic steatosis due to reduced production of oleic acid[21]. In addition, intestine-specific *Scd1*-null mice were demonstrated to be more susceptible to inflammation and tumorigenesis in the intestine due to a deficiency of oleic acid[22]. Notably, adipose-specific *Scd1*-null mice, liver-specific *Scd1*-null mice, and mice deficient in both adipose and liver SCD1 were not protected from HFD-induced obesity, despite reduced levels of MUFA, the products of SCD1 metabolism, being found in both subcutaneous and epididymal white adipose tissue[23]. However, until now, whether intestinal SCD1 contributes to the obesity-resistant phenotype remains unclear, and there are still no studies that examine the pharmacological contribution of tissue-specific SCD1, to metabolic disorders. Notably, efforts have been made to develop inhibitors targeting liver SCD1 for the treatment of metabolic disorders, such as MK-8245 for diabetes and aramchol for metabolic dysfunction-associated steatohepatitis[24,25]. Paradoxically, preclinical studies show that SCD1 expressed in the liver fails to modulate the obesity[21,23], which questions whether it is reasonable to target hepatic SCD1 for treating obesity-associated metabolic disorders. Studying how tissue-specific SCD1 determines the progression of HFD-induced obesity, and the anti-obesity effect produced by chemical SCD1 inhibition would be of great importance to help guide drug discovery targeting SCD1.

In the present study, intestinal *Scd1* mRNA was induced both in human and mice during obesity and intestine-specific *Scd1* deletion ameliorated HFD-induced obesity and hepatic steatosis, at least partially through inducing metallothionein 1 (MT1) to protect the intestine from oxidative stress. Notably, pharmacological inhibition of SCD1 by A939572 improved HFD-induced obesity and hepatic steatosis dependent on the presence of intestinal, but not hepatic, SCD1, highlighting intestinal SCD1 as a potential target for treating obesity.

2. Materials and methods

2.1. Mouse studies

Scd1-floxed ($Scd1^{fl/fl}$)[21] mice, Alb-cre, Villin-cre and Villin-ERT2-cre mice were previously described[26,27]. Alb-cre $Scd1^{fl/fl}$ ($Scd1^{\Delta Hep}$) mice and Villin-cre $Scd1^{fl/fl}$ ($Scd1^{\Delta IE}$) mice were generated by breeding $Scd1^{fl/fl}$ mice with Alb-cre mice and Villin-cre mice, respectively. For temporal intestine-specific disruption, villin-ERT2-cre $Scd1^{fl/fl}$ ($Scd1^{\Delta IE,ERT2}$) mice were generated by breeding $Scd1^{fl/fl}$ mice with villin-ERT2-cre mice. To activate the ERT2-cre,

the mice were first injected intraperitoneally with 50 mg/kg (body weight) tamoxifen (dissolved in corn oil, Sigma, St. Louis, MO, USA) for three consecutive days, which were followed by administration of 50 mg/kg (body weight) tamoxifen by intraperitoneal injection once weekly until the end of the study. HFD (60 kcal% from fat) was purchased from Bio-Serv (Cat#S3282, Flemington, NJ, USA). Male 7- to 8-week-old littermates were fed a chow diet or HFD for the indicated times to induce obesity and hepatic steatosis. For the lipid absorption study, 1-week HFD fed *Scd1*$^{fl/fl}$ and *Scd1*$^{\Delta IE}$ mice were fasted for 16 h, followed by 500 mg/kg tyloxapol (Sigma, St. Louis, MO, USA) administration *via* intravenous injection. Thirty minutes later, the mice were orally dosed with 10 mL/kg corn oil (Sigma), and blood was collected at 0, 1, 2, 4 and 6 h after corn oil treatment. For the fecal pellet collection, each mouse was transferred to a separate container for 6 h and feces collected starting right after the dosage of corn oil that lasted until the end of the experiment. Fresh feces were dried and dissolved in isopropanol for non-esterified fatty acid (NEFA) measurement. At the end of the experiment, the mice were euthanized to collect ileum tissues, while these ileum tissues were homogenized in 50 mmol/L tris buffer containing 1% Triton X-100 for triglyceride (TG) measurement. For the NAC treatment experiment, male *Scd1*$^{fl/fl}$ and *Scd1*$^{\Delta IE}$ mice at 7- to 8-weeks old were fed a HFD and maintained on vehicle or 2 g/L NAC (Sigma, St. Louis, MO, USA) in the drinking water for 12 weeks. For the SCD1 inhibitor studies, A939572 (Med Chem Express, Monmouth Junction, NJ, USA) was suspended in saline with 0.5% sodium carboxymethyl cellulose, 2.5% Tween 80 and 2.5% DMSO, while 7- to 8-week-old male mice were administered control vehicle or 10 mg/kg (body weight) A939572 by gavage once daily while maintained on a HFD for indicated time. Mice were housed in a temperature-controlled room at 20−24 °C with average humidity of 40% under a standard 12-h light/12-h dark cycle with water and food provided ad libitum. All mouse studies were approved by the National Cancer Institute Animal Care and Use Committee and conducted in accordance with the Institute of Laboratory Animal Resources guidelines.

2.2. Human cohort

Mucosal biopsy samples of the distal ileum were taken from individuals during routine colonoscopy. The sexes and ages were at similar levels in the overweight group (body mass index (BMI) $\geq$ 23; n = 19) and control group (BMI <23; n = 5) according to World Health Organization standard for overweight in Asian population[28], with clinical variables listed in Supporting Information Table S1. All individuals met the following inclusion criteria: (1) no diabetic ketoacidosis or hyperglycemic hyperosmolar state; (2) decompensated cirrhosis; (3) decompensated cirrhosis; (4) stage 3−5 chronic kidney disease; (5) inflammatory bowel disease; (6) no cancer; (7) no pulmonary tuberculosis and acquired immunodeficiency syndrome; (8) no alcoholism; (9) no antibiotics (including rifaximin), probiotics, prebiotics, proton pump inhibitors, and laxatives taking during the last 3 months and (10) no disease as judged by clinicians as unsuitable for biopsy. Normal liver tissues were collected from hepatic hematoma patients during surgery. All individuals with cancer and viral hepatitis type B were excluded, with clinical variables listed in Supporting Information Table S2. The study was approved by the Ethics Committee of Third Hospital, Peking University with protocol number LM2024507, and all individuals were given written informed consent before participating in the study.

2.3. Quantitative real-time PCR

Total RNA was extracted from liver or intestine tissues by using TRIzol (Invitrogen, Waltham, MA, USA). cDNA was synthesized from 1 μg of total RNA using qScript cDNA SuperMix (Quantabio, Beverly, MA, USA). Analysis was performed by using the ABI PRISM 7900 Sequence Detection System (Applied Biosystems, Bedford, MA, USA). The relative amount of each mRNA was calculated by normalizing to their corresponding *Actb* or *Gapdh* mRNAs, with the results expressed as fold change values relative to the control group. Real-time PCR primer sequences are listed in Supporting Information Table S3.

2.4. Metabolic assays

For the glucose-tolerance test, mice were dosed with glucose (2 g/kg) in saline *via* intraperitoneal injection after a 16-h fasting. For the insulin-tolerance test, the mice were fasted for 6 h and injected intraperitoneally with insulin (Eli Lilly, Indianapolis, IN, USA; 0.9 U/kg) in saline. For both glucose-tolerance test and insulin-tolerance test, blood glucose in the tail vein was measured at 0, 15, 30, 60, 90 and 120 min after injection by using a glucometer (Bayer, Washington D.C., USA).

2.5. Histological analysis

Formalin-fixed paraffin-embedded liver and intestine sections were stained by hematoxylin and eosin (H&E). Optimal cutting temperature compound-embedded frozen liver sections were stained with oil red O by following standard protocols and subjected to microscopic examination.

2.6. Lipid analysis

Serum and hepatic triglyceride, cholesterol and non-esterified fatty acid levels were measured by using assay kits from Wako Diagnostics (Wako Chemicals, Richmond, VA, USA) according to the manufacturer's instructions.

2.7. Serum aminotransferase assay

Alanine transaminase (ALT) and aspartate transferase (AST) levels were assessed in a 96-well microplate using commercial assay kits (Catachem, Oxford, MS, USA) and monitored at 340 nm by a kinetic reading with 30 s interval for 15 min by using a microplate reader (BioAssay Systems).

2.8. Oxidative stress assay

The levels of lipid peroxidation in mouse ileum tissues and serum were measured using the thiobarbituric acid reactive substances assay kit (Cayman Chemical, Ann Arbor, MI, USA) following the manufacturer's protocol. The total glutathione (GSH) levels in mouse ileum tissues and serum were measured using the glutathione assay kit from Sigma in accordance with the manufacturer's instructions. The ROS levels in MC38 cells and mouse primary intestinal epithelial cells were determined by using the dichlorodihydrofluorescein diacetate assay kit (Abcam, Cambridge, UK).

2.9. Indirect calorimetry

Indirect calorimetry was performed on 4-week HFD-fed mice using a 12-chamber Environment Controlled CLAMS (Columbus Instruments, Columbus, OH, USA) with one mouse in each chamber as previously described[27]. Mice were tested every 13 min for 3 days at 22 °C and 1 day at 30 °C. The temperature was changed on Day 4. Food and water were provided ad libitum during testing. 24 h average parameters were analyzed from data collected on Day 3 for 22 °C and Day 4 for 30 °C (excluding the first hour after temperature changes).

2.10. RNA-seq library preparation and data analysis

Total RNA was extracted from mouse jejunum and ileum using RNeasy Plus Mini Kit (Qiagen, Germantown, MD, USA) according to the manufacturer's instructions. RNA-seq libraries were prepared using Illumina TruSeq Stranded mRNA Library Prep (Illumina, San Diego, CA, USA). Samples were pooled and sequenced on a HiSeq 4000 (Illumina, San Diego, CA, USA) using a paired-end protocol. For RNA-seq data analysis, reads of the samples were trimmed for adaptors and low-quality bases using Trimmomatic 0.36 software before alignment with the mouse reference genome (mm10) and the annotated transcripts using STAR 2.5.1. The mapping statistics were calculated using Picard 1.84 software. Library complexity was measured in terms of unique fragments in the mapped reads using Picard's MarkDuplicate utility. The gene expression quantification analysis was performed for all samples using STAR/RSEM 1.2.22 tools. Differential gene expression was assessed with DESeq2 using the parameters adjusted P value of 0.05 and log2 fold change of 1 (for 2-fold differentially expressed genes). The RNA-Seq data were deposited in NCBI's Gene expression Omnibus with GEO Series accession number GSE272268.

2.11. Mass spectrometry-based analysis

Total fatty acids were analyzed after acid hydrolysis and quantified by using an Agilent 8890 gas chromatograph (8890 GC system) coupled with a 5977B GC/mass-selective detector (MSD) (Agilent Technologies, Santa Clara, CA, USA) as previously described[27]. In brief, 50 μL of serum were mixed with 400 μL acetonitrile and 400 μL CH_2Cl_2 containing 20 μmol/L of myristic-d27 acid as internal standard (Sigma), and centrifuged at 18,000×g for 10 min. The supernatant (750 μL) was transferred to a new tube and dried under vacuum. The dried samples were resuspended in 300 μL of hydrogen chloride−methanol solution (Sigma) and transferred to a glass bottle. After 60-min incubation at 100 °C, 300 μL hexane was added to extract the formed fatty acid esters and 100 μL supernatant was used for injection. For liver or intestine tissues, 20 mg samples were used and processed similarly as the serum samples, except that after extraction with hexane followed by as centrifugation, 500 μL supernatant was transferred to a new tube and dried under a stream of nitrogen and resuspended with 200 μL hexane for injection. Fatty acid standards were purchased from Sigma. The GC−MS chromatography was performed on a Supelco SP-2560 fused silica capillary column (100 m × 0.250 mm, 0.20 μm; Sigma−Aldrich, St. Louis, MO, USA), with GC−MS chromatographic and detection parameters as follows: initial oven temperature at 100 °C for 3 min, increasing to 200 °C at 3 °C/min holding for 3 min, then finally increasing to 240 °C at 3 °C/min with 6 min hold time for total 59 min run time. The front inlet temperature was 200 °C operating in splitless mode. Helium was used as the carrier gas at a constant flow of 1.65 mL/min. Samples and standards were injected onto the GC column at 1 μL. MSD transfer line, ion source and interface temperatures were 240, 230 and 280 °C, respectively. The MSD operated in EI scan mode at 70 eV. Extracted ions from the scan data were used for the quantitative analyses, as previously described[27]. The data were acquired and processed using Agilent MassHunter WorkStation Quantitative analyses version 10.1 software (Agilent Technologies, Santa Clara, CA, USA).

Serum, liver and intestinal bile acid metabolites were analyzed by using LC−MS/MS as previously described[27]. In brief, 25 μL serum or about 20 mg liver or intestine tissues were homogenized in 500 μL acetonitrile containing 1 μmol/L ursodeoxycholic acid-d_4 (Sigma) as internal standard and centrifuged at 14,000 rpm (Beckman Coulter Microfuge 20 Centrifuge, Beckman Coulter, Brea, CA, USA) for 10 min. The supernatant (150 μL) was transferred to a new tube and dried using a speed vacuum. The dried samples were suspended in 200 μL 30% methanol (methanol:water = 3:7, v/v) and vortexed for 30 s. After centrifuged at 12,000 rpm (Beckman Coulter Microfuge 20 Centrifuge, Beckman Coulter, Brea, CA, USA) for 10 min, the supernatant was transferred to a vial for LC−MS/MS injection. Bile acids were detected by a Waters Acquity I-Class UPLC/Synapt-G2Si QTOFMS system, as previously described[27].

2.12. Intestinal epithelial cells isolation and treatment

Primary intestinal epithelial cells were isolated from 1-week HFD treated *Scd1*$^{fl/fl}$ and *Scd1*$^{\Delta IE}$ mice as previously reported[29,30], seeded on collagen I-coated 12-well plates, and cultured with Dulbecco's modified Eagle's medium/F12 containing 10% fetal bovine serum, 1% antibiotics (GeminiBio, West Sacramento, CA, USA), 1% insulin-transferrin-sodium (ThermoFisher, Pittsburg, KS, USA), 500 ng/mL of R-spondin 1 (PeproTech, Cranbury, NJ, USA), 100 ng/mL of noggin (PeproTech, Cranbury, NJ, USA), 50 ng/mL of epidermal growth factor (PeproTech) and 10 μmol/L Y27632 (Selleck Chem, Houston, TX, USA). The primary intestinal epithelial cells were treated with scramble shRNA or *Mt1*-shRNA, or recombinant *Mt1* plasmid or matched control empty vector plasmid (FLAG-HA-pcDNA 3.1, Addgene plasmid # 52535, RRID: Addgene_52535), and collected 48 h post-treatment.

2.13. Western blot

Tissues were lysed with RIPA lysis buffer in the presence of protease inhibitors, followed by protein concentrations determination by the BCA protein assay kit (Pierce Chemical, Rockford, IL, USA). The samples were subjected to SDS-polyacrylamide gel electrophoresis, and transferred to polyvinylidene fluoride membranes, followed by incubation overnight at 4 °C with antibodies against SCD1 (Cell Signaling Technology, Danvers, MA, USA), β-actin (ACTB, Abclonal, Woburn, MA, USA), and MT1 (LSBio, Shirley, MA, USA). Proteins were visualized using the SuperSignalTM West Dura Extended Duration Substrate (ThermoFisher) with an image analyzer (Alpha Innotech Corp., San Leandro, CA, USA).

2.14. Statistics and reproducibility

Statistical analysis was performed by using Prism version 9.3.1 (GraphPad software). Experimental values are presented as the mean ± standard error of mean (SEM). A two-tailed Student's

t-test was used for two-group comparisons. One-way ANOVA followed by Tukey's multiple-comparisons test or two-way ANOVA followed by Tukey's multiple-comparisons test was employed to determine the statistical significance among multiple groups as described in the Figure legends. Correlation was assessed by using non-parametric Spearman's test. *P* values were calculated with 95% confidence intervals, and statistically significant differences were considered at $P < 0.05$.

3. Results

3.1. Intestinal SCD in human and SCD1 in mouse is induced by obesity

To investigate the potential association between intestinal human SCD (homologous to mouse SCD1) and obesity, *SCD* mRNA expression in human was quantified in distal ileum biopsies from individuals with or without obesity. Higher levels of *SCD* mRNA were observed in overweight individuals relative to lean controls (Fig. 1A). The *SCD* mRNA levels in the ileum were positively correlated with BMI (Fig. 1B). Consistent with the human data from the ileum, ileum *Scd1* mRNA was significantly induced in 3-week HFD-fed mice as well as in 10-week HFD-fed mice (Fig. 1C and D). No significant difference was observed in the liver *SCD* mRNA between the overweight individuals and the lean controls (Supporting Information Fig. S1A), while the liver *SCD* mRNA levels also did not significantly correlate with BMI in humans (Fig. S1B). In line with the human data, the liver *Scd1* mRNA was not significantly changed in 3-week and 10-week HFD-fed mice (Fig. S1C and S1D). These data demonstrate that obesity induces the expression of intestinal, but not the hepatic, SCD1.

3.2. Intestinal Scd1 deficiency improves obesity and fatty liver

To explore the role of intestinal SCD1 in obesity-associated metabolic disorders, an intestine-specific *Scd1*-disrupted mouse line ($Scd1^{\Delta IE}$) was generated. *Scd1* mRNA and SCD1 protein levels were largely reduced in the intestines of $Scd1^{\Delta IE}$ mice compared to $Scd1^{fl/fl}$ mice, with no change in *Scd1* mRNA levels in the liver (Supporting Information Fig. S2A–S2F). H&E staining of the small intestine revealed a similar morphology between $Scd1^{fl/fl}$ mice and $Scd1^{\Delta IE}$ mice (Fig. S2G), indicating no significant histological damage caused by intestinal *Scd1* disruption.

$Scd1^{\Delta IE}$ mice displayed less body weights, liver weights and liver indexes compared to $Scd1^{fl/fl}$ mice under HFD feeding (Fig. 2A–C). Glucose tolerance test (GTT) and insulin tolerance test (ITT) indicated that intestinal *Scd1* disruption substantially improved glucose tolerance and insulin sensitivity (Fig. 2D–G). Serum ALT and AST levels, serum and hepatic total cholesterol (TC) levels, and hepatic TG levels were markedly lower in $Scd1^{\Delta IE}$ mice, with no significant difference in serum triglyceride levels and hepatic NEFA levels between $Scd1^{fl/fl}$ mice and $Scd1^{\Delta IE}$ mice (Fig. 2H–N). Reduced hepatic lipid droplets in $Scd1^{\Delta IE}$ mice was revealed by H&E and oil red O staining (Fig. 2O and P). As TG could be formed from lipogenesis and consumed through glycolysis and gluconeogenesis, amelioration of these HFD-induced adverse metabolic phenotypes was correlated with reduced mRNA levels of the lipogenesis-related gene *Srebp1c*, and increased mRNA expression of genes involved in glycolysis and gluconeogenesis in the livers of $Scd1^{\Delta IE}$ mice compared with $Scd1^{fl/fl}$ mice, with no significant difference observed in mRNAs encoding fatty acid β-oxidation enzymes between the two genotypes (Supporting Information Fig. S3A–S3D). $Scd1^{\Delta IE}$ mice exhibited enhanced energy expenditure and higher oxygen consumption at both 22 °C and 30 °C compared to $Scd1^{fl/fl}$ mice. The respiratory exchange ratio was also increased in $Scd1^{\Delta IE}$ mice, which indicates increased glucose utilization probably due to increased muscle insulin sensitivity, with no changes in total activity (Fig. S2H–S2L). Increased *Ucp1* mRNA levels were found in the subcutaneous white adipose tissue of $Scd1^{\Delta IE}$ mice (Fig. S2M), indicating enhanced thermogenesis in these mice. To further explore if the improved phenotype sustains under longer HFD treatment, $Scd1^{fl/fl}$ and $Scd1^{\Delta IE}$ mice were subjected to extended HFD feeding for 15 weeks. $Scd1^{\Delta IE}$ mice exhibited lower body weights and liver weights, and less hepatic lipid accumulation compared to $Scd1^{fl/fl}$ mice after 15 weeks of HFD feeding (Supporting Information Fig. S4A–S4Q). These data demonstrate that intestinal *Scd1* disruption maintains an anti-obesity phenotype in mice fed a HFD for an extended duration. Furthermore, intestinal SCD1 deficiency improved obesity-associated metabolic disorders even under an 18-month chow diet feeding during long-term aging, as indicated by decreased body weights and improved insulin sensitivity, glucose tolerance and hepatic lipid profiles (Supporting Information Fig. S5A–S5Q), suggesting that intestinal SCD1 deficiency could protect mice from aging-accompanied obesity. These data demonstrate that intestinal SCD1 expression contributes to obesity progression during HFD feeding.

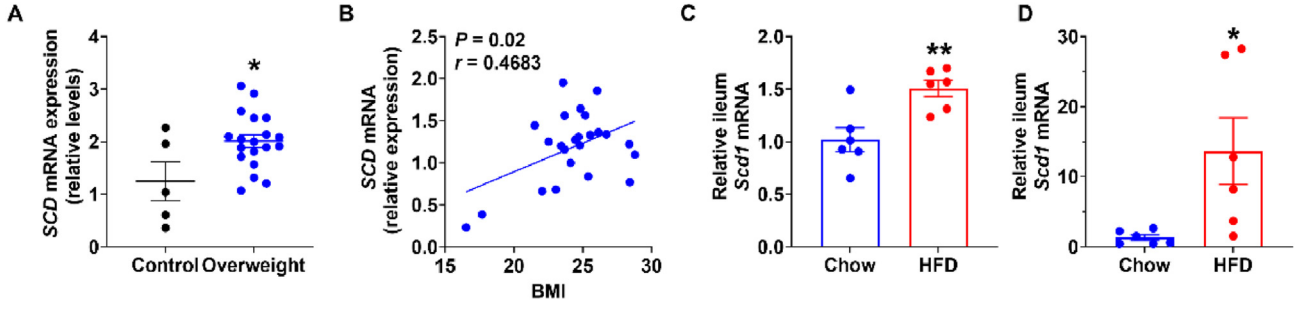

Figure 1 SCD1 was induced in the small intestines of humans and mice with obesity. (A) mRNA levels of *SCD* in the ileum biopsies from individuals with obesity ($n = 19$) or without obesity ($n = 5$). (B) Correlation of *SCD* mRNA levels with body mass index (BMI); $n = 24$. (C, D) *Scd1* mRNA levels in the ileum of C57BL/6N mice fed a chow diet or high-fat diet (HFD) for 3 weeks (C) or 10 weeks (D); $n = 6$. All data are presented as the mean ± SEM of biologically independent samples, analyzed by a two-tailed student's *t*-test (A, C and D) or a non-parametric Spearman's test (B). $^*P < 0.05$, $^{**}P < 0.01$, overweight *versus* control or HFD *versus* chow.

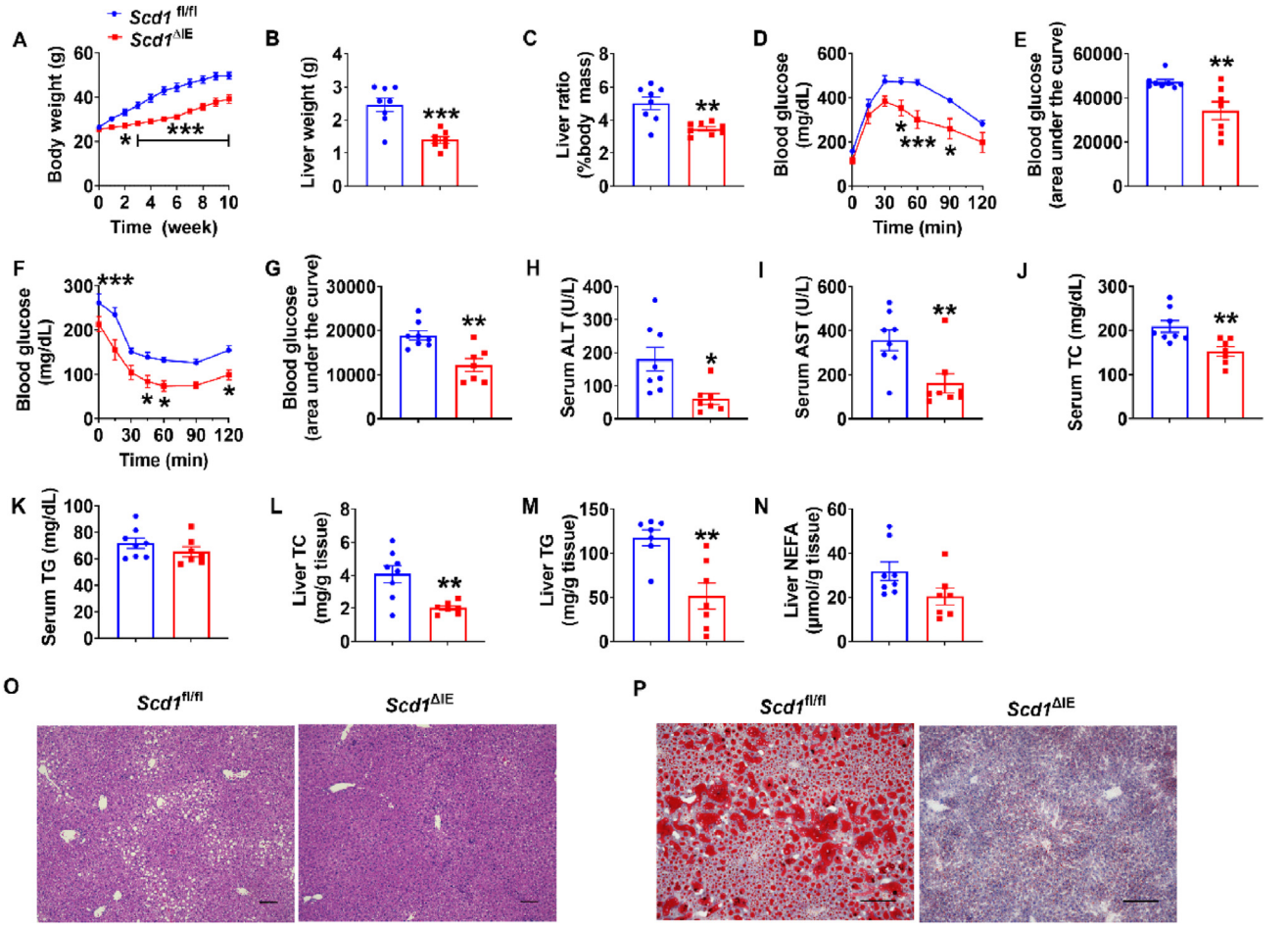

Figure 2 *Scd1*$^{\Delta IE}$ mice displayed less obesity and hepatic steatosis under high-fat diet challenge. *Scd1*$^{fl/fl}$ and *Scd1*$^{\Delta IE}$ mice were fed a chow diet or high-fat diet for 10 weeks; $n = 8$ for *Scd1*$^{fl/fl}$ group and $n = 7$ for *Scd1*$^{\Delta IE}$ group. (A) Body weight curves. (B) Liver weights. (C) Liver index. (D, E) Glucose tolerance test (GTT) (D) and quantitation of area under the curve (E). (F, G) Insulin tolerance test (ITT) (F) and quantitation of area under the curve (G). (H) Serum alanine aminotransferase (ALT). (I) Serum aspartate aminotransferase (AST). (J) Serum total cholesterol (TC). (K) Serum triglyceride (TG). (L) Liver TC. (M) Liver TG. (N) Liver non-esterified fatty acid (NEFA). (O, P) Representative hematoxylin and eosin staining (O) and oil red O staining (P) of liver sections ($n = 3$ mice per group, three images per mouse per staining). Scale bar, 100 μm. All data are presented as the mean ± SEM of biologically independent samples, analyzed by a two-tailed student's *t*-test (B, C, E, G, H–N) or two-way ANOVA followed by Tukey's multiple comparisons test (A, D, F). *$P < 0.05$, **$P < 0.01$, ***$P < 0.001$, *Scd1*$^{\Delta IE}$ *versus* *Scd1*$^{fl/fl}$.

Since SCD1 is well-known to be expressed in hepatocytes, the possibility that hepatocyte SCD1 influences obesity-associated metabolic disorders was explored. To answer this question, hepatocyte-specific *Scd1* knockout (*Scd1*$^{\Delta Hep}$) mice were generated by breeding the *Scd1*$^{fl/fl}$ with the Alb-cre mice. However, no notable change in body weights, liver weights, liver indexes, glucose and insulin tolerance, serum and hepatic biochemical parameters or hepatic lipid accumulation was found in *Scd1*$^{\Delta Hep}$ mice compared to that in *Scd1*$^{fl/fl}$ mice (Supporting Information Fig. S6). These data suggest a minor role for hepatocyte SCD1 in modulating obesity-associated metabolic disorders during the challenge of HFD feeding.

3.3. *Intestinal Scd1 disruption induces MT1 expression*

Given that the main physiological role of SCD1 is to catalyze the desaturation of endogenous and exogenous saturated fatty acids to form the respective monounsaturated fatty acids, fatty acid composition in the intestine and serum of *Scd1*$^{fl/fl}$ and *Scd1*$^{\Delta IE}$ mice after 4-week or 10-week HFD feeding was analyzed. Unexpectedly, no notable change in fatty acid levels, including the substrates (C16:0 and C18:0) and products (C16:1 and C18:1) of SCD1, was found in either the intestine or the serum of *Scd1*$^{\Delta IE}$ mice under short- or long-term HFD treatment (Supporting Information Fig. S7A–S7D), while decreased levels of C16:1 and C18:1 were observed in the liver of *Scd1*$^{\Delta IE}$ mice fed a HFD for 10 weeks compared to *Scd1*$^{fl/fl}$ mice (Fig. S7E). These data indicate that the effect of intestinal SCD1 in *de novo* lipogenesis may not be a key causal factor that contributes to the metabolic phenotype. To further explore the effects of intestinal SCD1 deficiency on lipid absorption, serum TG and fecal NEFA levels were measured in *Scd1*$^{fl/fl}$ and *Scd1*$^{\Delta IE}$ mice challenged with corn oil. There was no significant difference in both the serum TG and fecal NEFA levels between the two genotypes (Fig. S7F and S7G), indicating that lipid absorption was not changed when SCD1 is knocked out in the intestine. Furthermore, TG levels in the intestine were unchanged between the *Scd1*$^{fl/fl}$ and *Scd1*$^{\Delta IE}$ mice (Fig. S7H), suggesting no change in TG synthesis in the intestine upon loss of intestinal SCD1.

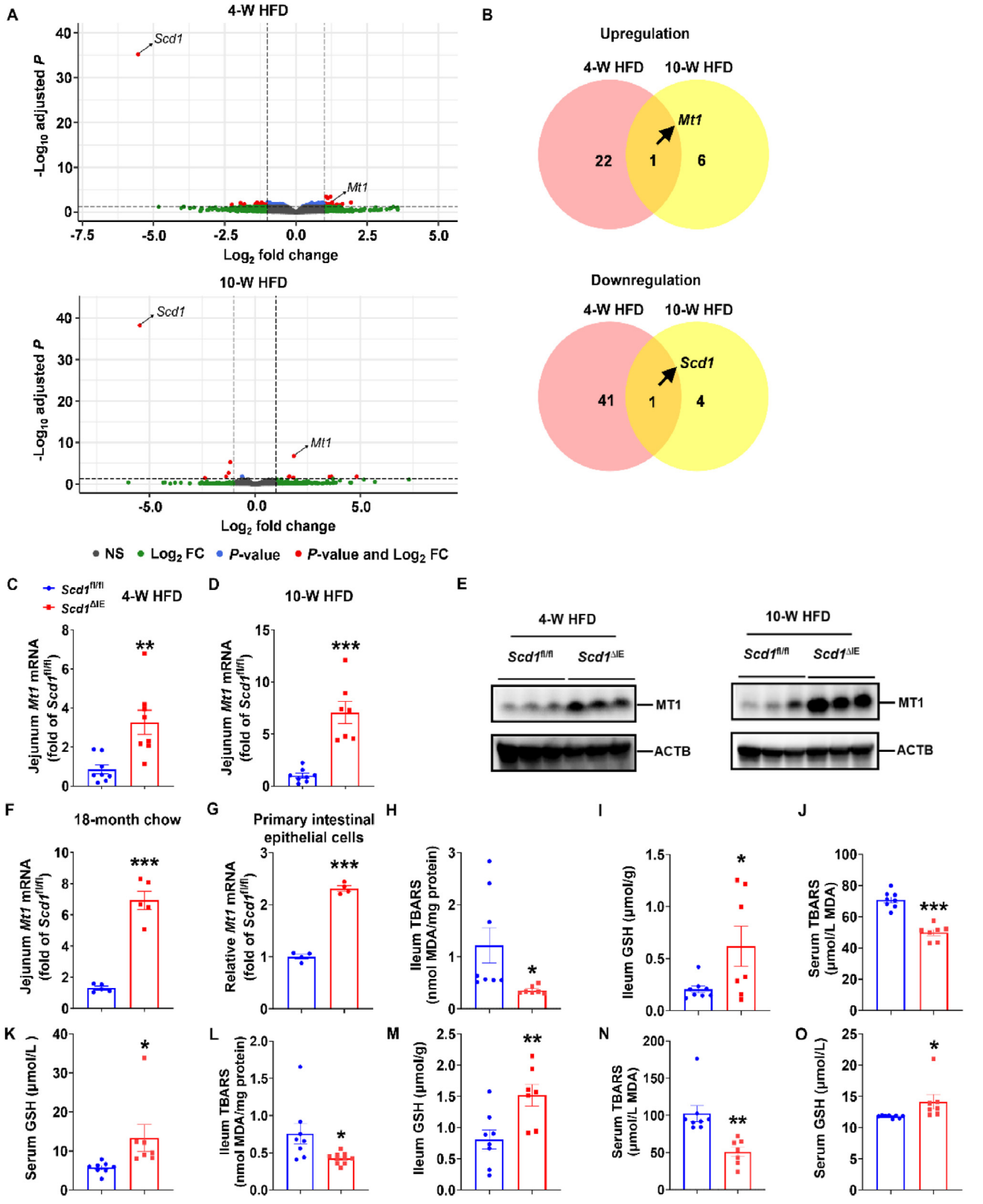

Figure 3 Intestinal *Scd1* disruption increased *Mt1* expression. (A, B) RNA-seq analysis of $Scd1^{fl/fl}$ and $Scd1^{\Delta IE}$ mice fed a high-fat diet (HFD) for 4 or 10 weeks. The volcano plot (A), and Venn plot (B) of the RNA-seq data from the intestines of $Scd1^{fl/fl}$ and $Scd1^{\Delta IE}$ mice fed a HFD for 4 weeks or 10 weeks. (C−E) mRNA levels of *Mt1* (C, D) and MT1 protein levels (E) in the jejunum of $Scd1^{fl/fl}$ and $Scd1^{\Delta IE}$ mice fed a HFD for 4 weeks or 10 weeks; (F) mRNA levels of *Mt1* in the jejunum of $Scd1^{fl/fl}$ and $Scd1^{\Delta IE}$ mice fed with chow diet for 18 months; $n = 8$ for 4-week and 10-week HFD fed $Scd1^{fl/fl}$ group, $n = 7$ for 4-week and 10-week HFD fed $Scd1^{\Delta IE}$ group, $n = 5$ for 18-month chow fed $Scd1^{fl/fl}$ and $Scd1^{\Delta IE}$ groups. (G) mRNA levels of *Mt1* in the primary intestinal epithelial cells isolated from $Scd1^{fl/fl}$ and $Scd1^{\Delta IE}$ mice fed a HFD for 2 weeks; $n = 3$.

Increased bile acids were found in the circulation in skin epidermis-specific *Scd1*-null mice and in both the serum and the liver of intestine-specific *Scd1*-null mice. Among the changed bile acids, lithocholic acid, deoxycholic acid, chenodeoxycholic acid, cholic acid and tauroursodeoxycholic acid, which function as Takeda G protein-coupled receptor 5 (TGR5) activators, were suggested to contribute to the protective phenotype from HFD-induced obesity in these mice[31,32]. To explore whether the obesity-resistant phenotype is also due to bile acid metabolite levels that were changed by intestinal *Scd1* disruption, serum, liver and ileum bile acid levels were then measured in 10-week HFD-fed $Scd1^{fl/fl}$ and $Scd1^{\Delta IE}$ mice. While no statistical difference was observed in bile acid levels in the ileum between $Scd1^{fl/fl}$ and $Scd1^{\Delta IE}$ mice (Supporting Information Fig. S8A), deoxycholic acid, hyodeoxycholic acid, lithocholic acid and taurolithocholic acid in the serum, and taurocholic acid, chenodeoxycholic acid, taurodeoxycholic acid, tauroursodeoxycholic acid and taurolithocholic acid in the liver were significantly decreased in 10-week HFD-treated $Scd1^{\Delta IE}$ mice compared to $Scd1^{fl/fl}$ mice (Fig. S8B and S8C). The total bile acids in the serum, liver and ileum, and the mRNA levels of bile acid synthesis and transport-related genes in the liver, as wells as genes related to bile acid uptake in the ileum, were not significantly changed between $Scd1^{fl/fl}$ and $Scd1^{\Delta IE}$ mice (Fig. S8D−S8H). These data suggest that the improved obesity phenotype in the $Scd1^{\Delta IE}$ mice in this study may not be meditated by bile acid changes and TGR5 activation.

Given that changes in metabolic profiles of both fatty acids and bile acids might not contribute to the observed obesity-resistant phenotype of $Scd1^{\Delta IE}$ mice, RNA-seq analysis was employed to explore the potential mechanisms underlying improved metabolic syndrome mediated by intestinal *Scd1* disruption. RNA-seq analysis was carried out on RNAs from the jejunum of $Scd1^{fl/fl}$ and $Scd1^{\Delta IE}$ mice fed a HFD for 4 weeks and 10 weeks. The differentially-expressed gene profiles between the two genotypes across the two experiments were analyzed using Volcano plots and overlapped using Venn diagram (Fig. 3A and B). In particular, *Mt1* mRNA was consistently increased by intestine-specific SCD1 deficiency, while *Scd1* mRNA was, as expected, decreased by intestinal *Scd1* disruption (Fig. 3A and B). Similar data were found in the RNA-seq analysis by using ileum samples from 3-week and 15-week HFD fed $Scd1^{fl/fl}$ and $Scd1^{\Delta IE}$ mice, as *Mt1* mRNA was increased and *Scd1* decreased by intestinal SCD1 deficiency under both feeding conditions (Supporting Information Fig. S9A and S9B), indicating that both the jejunum and ileum shared similar patterns of *Mt1* mRNA induction. Induction of *Mt1* mRNA was further confirmed by real-time quantitative polymerase chain reaction in $Scd1^{\Delta IE}$ mice fed chow or a 4-week or 10-week HFD or a 3-week or 15-week HFD (Fig. 3C, D and F, Fig. S9C and S9D), and the increase in MT1 protein was further confirmed by western blot analysis of intestine tissue from $Scd1^{fl/fl}$ and $Scd1^{\Delta IE}$ mice after 4-week or 10-week HFD feeding (Fig. 3E). Primary intestinal epithelial cells isolated from HFD-fed $Scd1^{\Delta IE}$ mice also displayed higher *Mt1* mRNA levels compared to that of $Scd1^{fl/fl}$ mice (Fig. 3G). These data demonstrate that intestinal *Scd1* disruption mainly causes the increased *Mt1* mRNA, primarily in epithelial cells.

3.4. *Intestinal Scd1 disruption restricts HFD-induced oxidative stress by inducing MT1 expression*

MT1 is involved in regulating oxidative stress by quenching ROS[33], suggesting that intestinal SCD1 deficiency may reduce obesity by decreasing obesity-induced oxidative stress. Since increased oxidative stress was previously shown to be involved in obesity[12], intestinal oxidative stress was examined in HFD-fed mice. Increased oxidative stress, as reflected by elevated malondialdehyde (MDA) and decreased GSH levels, was found in the ileum of C57BL/6N mice fed a HFD for 3 weeks or 10 weeks as compared to mice fed a chow diet (Fig. S9E−S9H). In line with the hypothesis that intestinal SCD1 may reduce oxidative stress, 3-week or 10-week HFD-fed $Scd1^{\Delta IE}$ mice exhibited markedly lower MDA and higher GSH levels in the ileum as well as in the serum compared to that of $Scd1^{fl/fl}$ mice (Fig. 3H−O). To further determine if decreased oxidative stress contributes to the decreased obesity induced by HFD in $Scd1^{\Delta IE}$ mice, NAC, an oxidative stress inhibitor, was used to treat $Scd1^{fl/fl}$ and $Scd1^{\Delta IE}$ mice fed a HFD. While intestinal *Scd1* disruption or NAC treatment decreased body weight and liver weight, improved insulin resistance, lowered serum ALT, AST and cholesterol levels, reduced hepatic lipid accumulation, and improved oxidative stress markers in the serum and ileum, these parameters were not further improved in $Scd1^{\Delta IE}$ mice treated with NAC compared to those in $Scd1^{\Delta IE}$ mice treated with vehicle (Fig. 4A−U), indicating that intestinal SCD1 deficiency protects mice from HFD-induced obesity at least partially through improving oxidative stress.

To further examine whether intestinal SCD1 deficiency-induced MT1 contributes to its effect in restricting oxidative stress, intestine-derived immortalized MC38 cells were treated with recombinant lentivirus carrying mouse *Mt1* shRNA to silence MT1 followed by palmitic acid challenge. Palmitic acid treatment significantly increased the levels of oxidative stress and reduced the *Mt1* mRNA expression, while *Mt1* shRNA-caused reduction of *Mt1* expression was found to increase the oxidative stress both in the presence and absence of palmitic acid treatment (Fig. 5A−D), indicating a role for MT1 in preventing oxidative stress in intestinal cells. To further examine whether MT1 induction contributes to the anti-oxidant role of intestinal SCD1 disruption, primary intestinal epithelial cells were isolated from 1-week HFD-fed $Scd1^{fl/fl}$ and $Scd1^{\Delta IE}$ mice. Higher *Mt1* mRNA levels accompanied by lower oxidative stress were found in intestinal epithelial cells from $Scd1^{\Delta IE}$ mice compared to those in $Scd1^{fl/fl}$ mice-derived cells, while the reduction of oxidative stress in the intestinal epithelial cells derived from $Scd1^{\Delta IE}$ mice was compromised when *Mt1* was silenced by lentivirus *Mt1* shRNA (Fig. 5E−H). Furthermore, mouse *Mt1* overexpression was found to decrease oxidative stress both in the presence and absence of palmitic acid treatment in primary intestinal epithelial cells (Fig. 5I−L). These data suggest that intestinal SCD1 disruption restricts intestinal oxidative stress at least partially by inducing the expression of MT1.

(H, I) Malondialdehyde (MDA) levels (H) and glutathione (GSH) levels (I) in the ileum of $Scd1^{fl/fl}$ and $Scd1^{\Delta IE}$ mice fed a HFD for 4 weeks. (J, K) MDA levels (J) and GSH levels (K) in the serum of $Scd1^{fl/fl}$ and $Scd1^{\Delta IE}$ mice fed a HFD for 4 weeks. (L, M) MDA levels (L) and GSH levels (M) in the ileum of $Scd1^{fl/fl}$ and $Scd1^{\Delta IE}$ mice fed a HFD for 10 weeks. (N, O) MDA levels (N) and GSH levels (O) in the serum of $Scd1^{fl/fl}$ and $Scd1^{\Delta IE}$ mice fed a HFD for 10 weeks. All data are presented as the mean ± SEM of biologically independent samples, analyzed by a two-tailed student's *t*-test (C, D, F−O). $*P < 0.05$, $**P < 0.01$, $***P < 0.001$, $Scd1^{\Delta IE}$ *versus* $Scd1^{fl/fl}$. TBARS, thiobarbituric acid reactive substances.

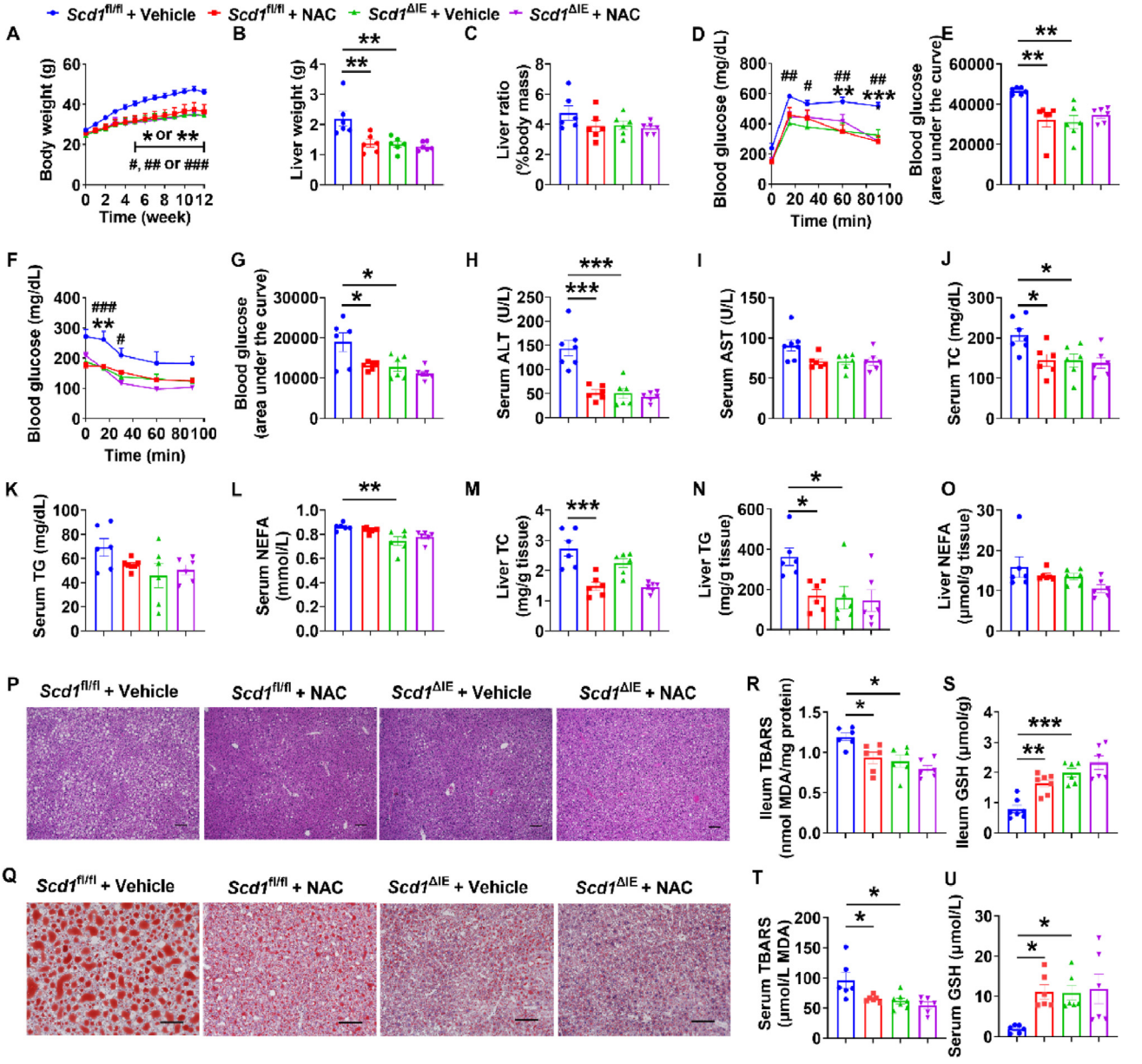

Figure 4 Intestinal *Scd1* disruption decreased obesity and fatty liver through reducing oxidative stress. $Scd1^{fl/fl}$ and $Scd1^{\Delta IE}$ mice were fed a high-fat diet and treated with vehicle or *N*-acetylcysteine (NAC) water (2 g/L) for 15 weeks, $n = 6$. (A) Body weight curve. (B) Liver weight. (C) Liver index. (D, E) Glucose tolerance test (GTT) (D) and quantitation of area under the curve (E). (F, G) Insulin tolerance test (ITT) (F) and quantitation of area under the curve (G). (H) Serum alanine aminotransferase (ALT). (I) Serum aspartate aminotransferase (AST). (J) Serum total cholesterol (TC). (K) Serum triglyceride (TG). (L) Serum non-esterified fatty acid (NEFA). (M) Liver TC. (N) Liver TG. (O) Liver NEFA. (P, Q) Representative hematoxylin and eosin staining (P) and oil red O staining (Q) of liver sections ($n = 3$ mice per group, three images per mouse per staining). Scale bar, 100 μm. (R–U) Malondialdehyde (MDA) and glutathione (GSH) levels in the ileum (R, S) and the serum (T, U) of $Scd1^{fl/fl}$ and $Scd1^{\Delta IE}$ mice fed a high-fat diet and treated with vehicle or NAC water. All data are presented as the mean ± SEM of biologically independent samples, analyzed using one-way ANOVA followed by Tukey's multiple comparisons test (B, C, E, G, O, R–U) or two-way ANOVA followed by Tukey's multiple comparisons test (A, D, F). (A, D, F) $^{*}P < 0.05$, $^{**}P < 0.01$, $^{***}P < 0.001$, $Scd1^{fl/fl}$ + NAC *versus* $Scd1^{fl/fl}$ + vehicle; $^{\#}P < 0.05$, $^{\#\#}P < 0.01$, $^{\#\#\#}P < 0.001$, $Scd1^{\Delta IE}$ + vehicle *versus* $Scd1^{fl/fl}$ + vehicle. (B, C, E, G, O, R–U) $^{*}P < 0.05$, $^{**}P < 0.01$, $^{***}P < 0.001$ *versus* the Control. TBARS, thiobarbituric acid reactive substances.

3.5. A939572 attenuates hepatic steatosis depending on the presence of intestinal SCD1

To further explore if the anti-obesity effect of chemical SCD1 inhibition on HFD-induced metabolic syndrome is dependent on the presence of intestinal SCD1 activity, A939572, a specific SCD1 inhibitor, was used to treat the $Scd1^{fl/fl}$ and $Scd1^{\Delta IE}$ mice fed a HFD for 12 weeks. Intestinal *Scd1* disruption or A939572 treatment decreased body weight and liver weight, improved insulin resistance, lowered serum ALT, AST and cholesterol levels, and reduced

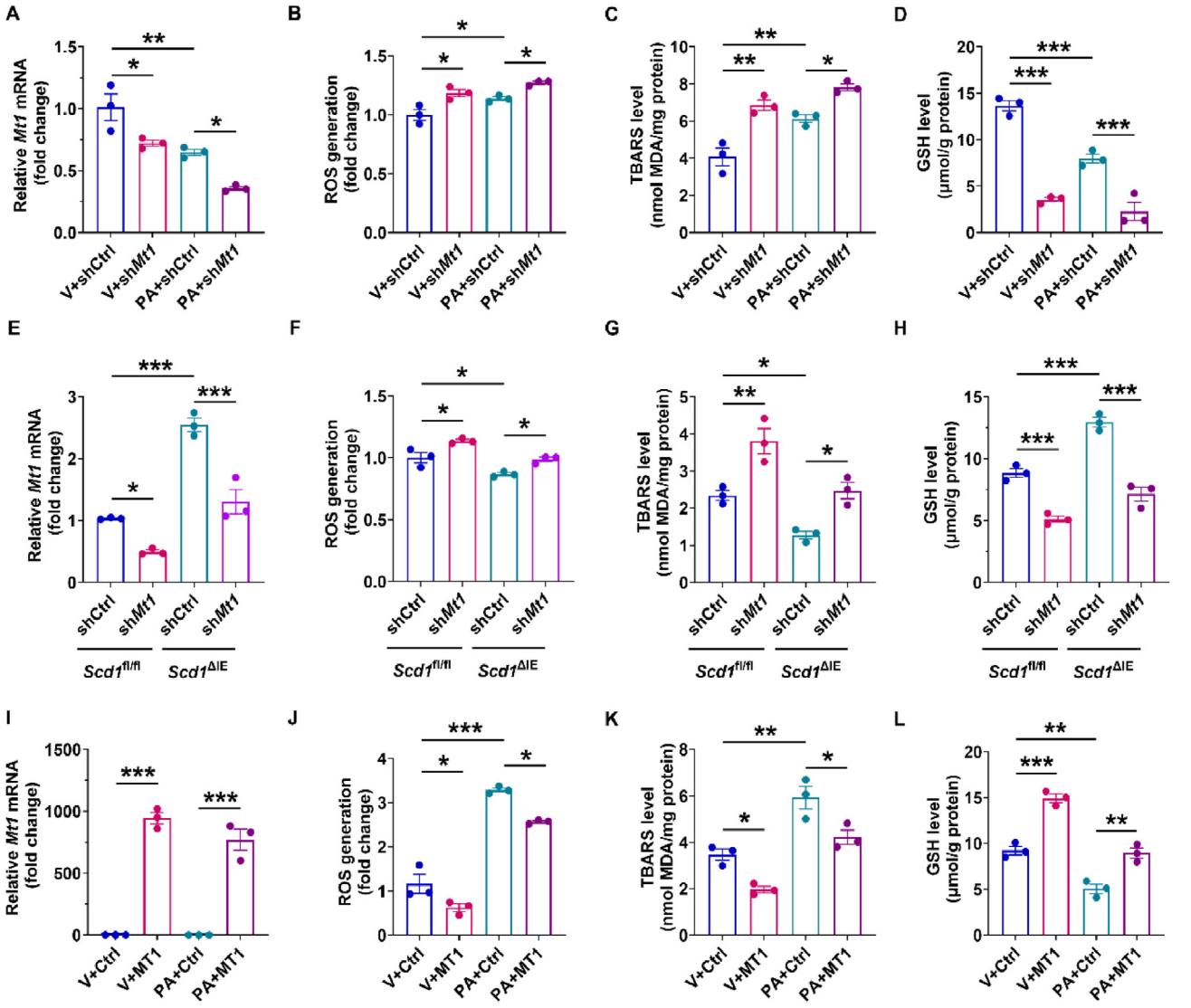

Figure 5 Intestinal SCD1 loss-induced *Mt1* upregulation contributed to the reduction of intestinal oxidative stress. (A−D) *Mt1* mRNA (A), reactive oxygen species (ROS) level (B), malondialdehyde (MDA) level (C) and glutathione (GSH) level (D) in MC38 cells treated with BSA control vehicle (V), BSA-conjugated 0.2 mmol/L palmitic acid (PA), scramble shRNA (shCtrl) or *Mt1*-shRNA (sh*Mt1*) as indicated. Cells were pretreated with scramble shRNA or *Mt1*-shRNA for 24 h and then treated with V or PA for another 24 h; $n = 3$. (E−H) *Mt1* mRNA (E), ROS levels (F), MDA levels (G) and GSH levels (H) in primary intestinal epithelial cells from $Scd1^{fl/fl}$ and $Scd1^{\Delta IE}$ mice treated with shCtrl or sh*Mt1* for 48h; $n = 3$. (I−L) *Mt1* mRNA (I), ROS level (J), MDA level (K) and GSH level (L) in primary intestinal epithelial cells from $Scd1^{fl/fl}$ and $Scd1^{\Delta IE}$ mice treated with BSA control vehicle (V), BSA-conjugated 0.2 mmol/L PA, control plasmid (Ctrl) or *Mt1*-overexpression plasmid (MT1) as indicated. Cells were pretreated with control plasmid or *Mt1*-overexpression plasmid for 48 h and then treated with V or PA for another 24 h; $n = 3$. All data are presented as the mean ± SEM of biologically independent samples, analyzed using one-way ANOVA followed by Tukey's multiple comparisons test. $^*P < 0.05$, $^{**}P < 0.01$, $^{***}P < 0.001$ *versus* the Control. TBARS, thiobarbituric acid reactive substances. TBARS, thiobarbituric acid reactive substances.

hepatic lipid accumulation (Fig. 6A−Q). However, $Scd1^{\Delta IE}$ mice treated with A939572 did not show further improvement in any of the metabolic parameters examined compared to those in $Scd1^{\Delta IE}$ mice treated with vehicle (Fig. 6A−Q), indicating that the effect of A939572 on HFD-induced metabolic syndrome was mainly dependent on the intact expression of intestinal SCD1. Increased MT1 and decreased oxidative stress were found in A939572-treated $Scd1^{fl/fl}$ mice, but no further increase of *Mt1* mRNA, or decrease of various markers of oxidative stress was observed in A939572-treated $Scd1^{\Delta IE}$ mice compared to $Scd1^{\Delta IE}$ mice after vehicle treatment (Fig. 6R−V), further supporting the view that decreased obesity in intestinal SCD1 knockout mice is at least partially due to reduced oxidative stress caused by MT1 induction.

A939572 was next employed to treat the HFD-fed $Scd1^{fl/fl}$ and $Scd1^{\Delta Hep}$ mice to examine whether A939572 reduced obesity and associated fatty liver depends on the presence of hepatic SCD1. The improved obesity and fatty liver in A939572-treated $Scd1^{fl/fl}$ mice were not different in $Scd1^{\Delta Hep}$ mice after A939572 treatment (Fig. 7A−Q), indicating that A939572 decreased HFD-induced obesity and hepatic steatosis in a hepatocyte SCD1-independent manner.

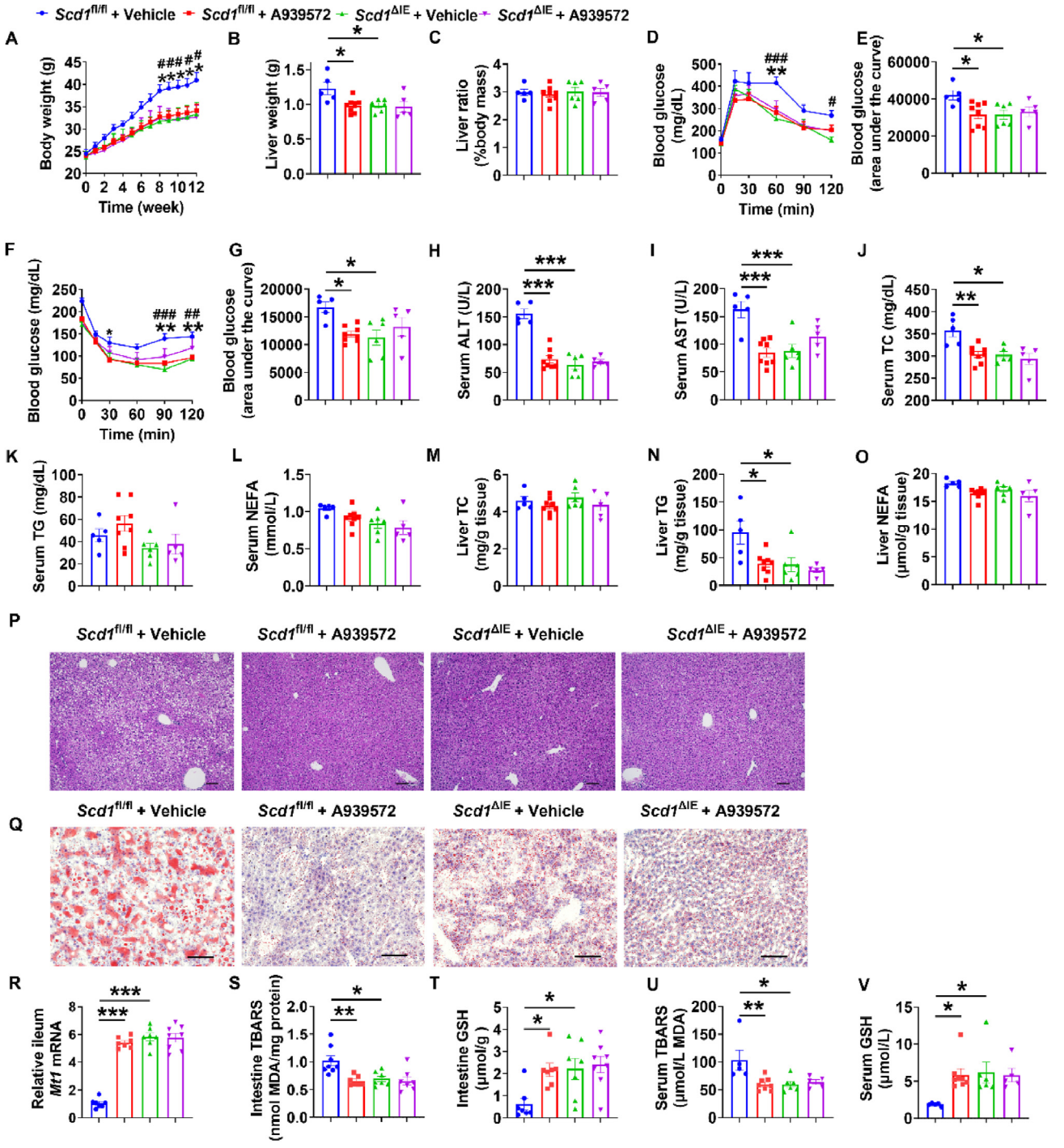

Figure 6 Chemical SCD1 inhibition improved high-fat diet-induced obesity and hepatic steatosis depending on the presence of intestinal SCD1. (A) Body weight curve. (B) Liver weight. (C) Liver index. (D, E) Glucose tolerance test (GTT) (D) and quantitation of area under the curve (E). (F, G) Insulin tolerance test (ITT) (F) and quantitation of area under the curve (G). (H) Serum alanine aminotransferase (ALT). (I) Serum aspartate aminotransferase (AST). (J) Serum total cholesterol (TC). (K) Serum triglyceride (TG). (L) Serum non-esterified fatty acid (NEFA). (M) Liver TC. (N) Liver TG. (O) Liver NEFA. (P, Q) Representative hematoxylin and eosin staining (P) and oil red O staining (Q) of liver sections ($n = 3$ mice per group, three images per mouse per staining). Scale bar, 100 μm. (R–V) *Mt1* mRNA (R), malondialdehyde (MDA) and glutathione (GSH) levels in the ileum (S, T) and the serum (U, V) of $Scd1^{fl/fl}$ and $Scd1^{\Delta IE}$ mice fed a high-fat diet for 12 weeks. $n = 5$ for $Scd1^{fl/fl}$ with vehicle group, $n = 8$ for $Scd1^{fl/fl}$ with A939572 group, $n = 6$ for $Scd1^{\Delta IE}$ with vehicle group, and $n = 5$ for $Scd1^{\Delta IE}$ with A939572 group. All data are presented as the mean ± SEM of biologically independent samples, analyzed using one-way ANOVA followed by Tukey's multiple comparisons test (B, C, E, G–O, R–V) or two-way ANOVA followed by Tukey's multiple comparisons test (A, D, F). (A, D, F) $^{*}P < 0.05$, $^{**}P < 0.01$, $Scd1^{fl/fl}$ + A939572 *versus* $Scd1^{fl/fl}$ + vehicle; $^{\#}P < 0.05$, $^{\#\#}P < 0.01$, $^{\#\#\#}P < 0.001$, $Scd1^{\Delta IE}$ + vehicle *versus* $Scd1^{fl/fl}$ + vehicle. (B, C, E, G–O, R–V) $^{*}P < 0.05$, $^{**}P < 0.01$, $^{***}P < 0.001$ *versus* the Control. TBARS, thiobarbituric acid reactive substances.

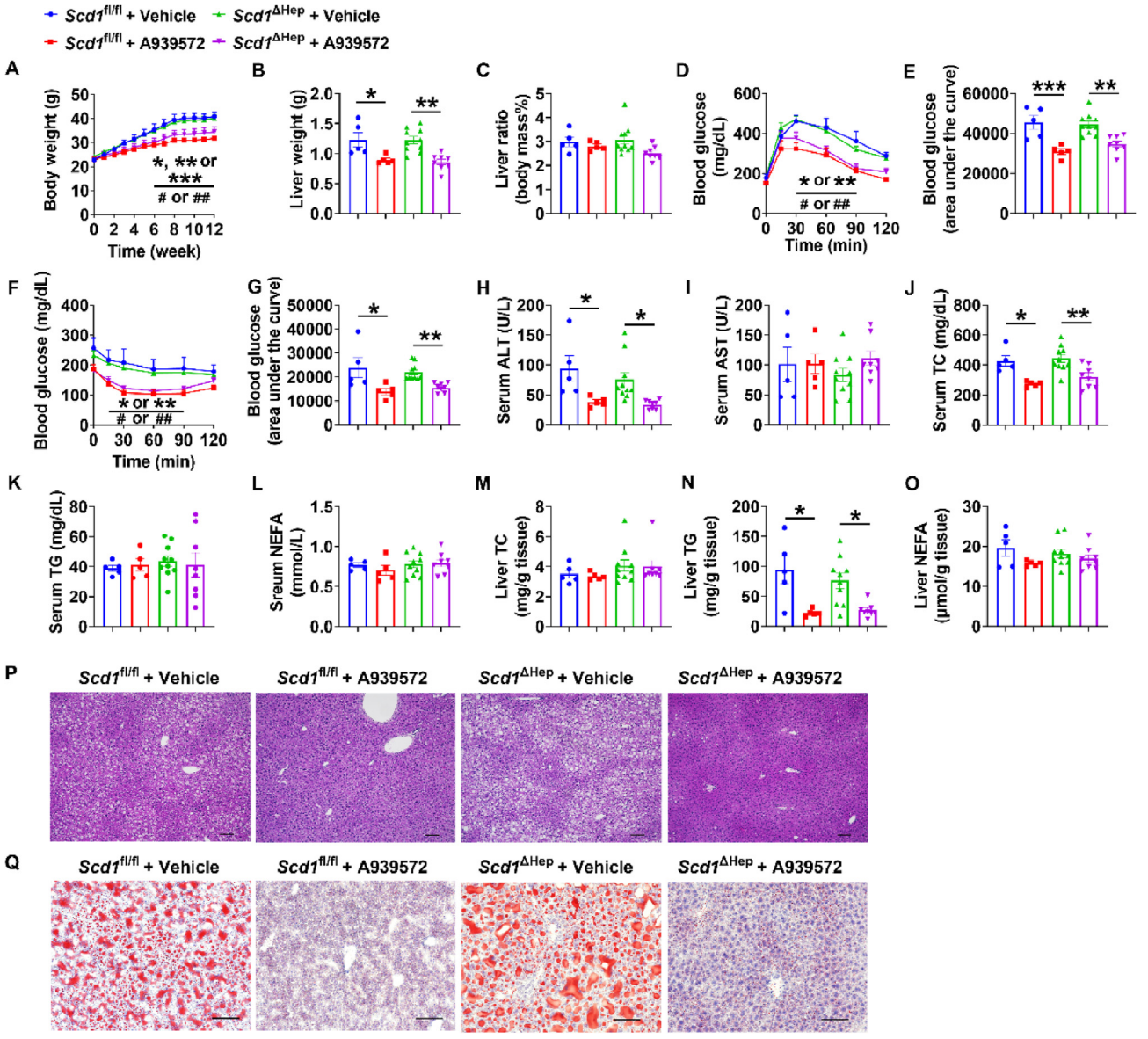

Figure 7 Improvement of hepatic steatosis induced by high-fat diet was independent of hepatic SCD1 inhibition. *Scd1*$^{fl/fl}$ and *Scd1*$^{\Delta Hep}$ mice were administered vehicle or A939572 while maintained on high-fat diet for 12 weeks. (A) Body weight curves. (B) Liver weights. (C) Liver index. (D) Glucose tolerance test (GTT). (E) GTT area under the curve. (F) Insulin tolerance test (ITT). (G) ITT area under the curve. (H) Serum alanine aminotransferase (ALT). (I) Serum aspartate aminotransferase (AST). (J) Serum total cholesterol (TC). (K) Serum triglyceride (TG). (L) Serum non-esterified fatty acid (NEFA). (M) Hepatic TC. (N) Hepatic TG. (O) Hepatic NEFA. (P, Q) Representative hematoxylin and eosin staining (P) and oil red O staining (Q) of liver sections ($n = 3$ mice per group, three images per mouse per staining). Scale bar, 100 μm. $n = 5$ for *Scd1*$^{fl/fl}$ with vehicle group and *Scd1*$^{fl/fl}$ with A939572 group, respectively, $n = 10$ for *Scd1*$^{\Delta Hep}$ with vehicle group, and $n = 8$ for *Scd1*$^{\Delta Hep}$ with A939572 group. All data are presented as the mean ± SEM of biologically independent samples, analyzed using one-way ANOVA followed by Tukey's multiple comparisons test (B, C, E, G, O) or two-way ANOVA followed by Tukey's multiple comparisons test (A, D, F). (A, D, F) */**/***$P < 0.05/0.01/0.001$, *Scd1*$^{fl/fl}$ + A939572 *versus* *Scd1*$^{fl/fl}$ + vehicle; $^{\#/\#\#}P < 0.05/0.01$, *Scd1*$^{\Delta Hep}$ + vehicle *versus* *Scd1*$^{fl/fl}$ + vehicle. (B, C, E, G, O) *$P < 0.05$, **$P < 0.01$, ***$P < 0.001$ *versus* the Control.

To further assess whether A939572-induced MT1 expression is a causal factor or a result of the A939572-caused anti-obesity phenotype, HFD-fed C57BL/6N mice treated with A939572 for 3 weeks were analyzed and *Mt1* mRNA was increased along with GSH levels concomitant with decreased MDA levels in the ileum, when the mouse body weights were not significantly changed by A939572 treatment (Supporting Information Fig. S10A−S10F). These data suggest that chemical SCD1 inhibition could induce MT1 expression at the early stage as an initial causal factor that likely contributes to its anti-obesity effect.

3.6. *Intestinal SCD1 disruption improves obesity and fatty liver in a therapeutic manner*

To further investigate if established obesity could be improved by intestinal SCD1 disruption, Villin-ERT2-cre *Scd1*$^{fl/fl}$ (*Scd1*$^{\Delta IE,ERT2}$)

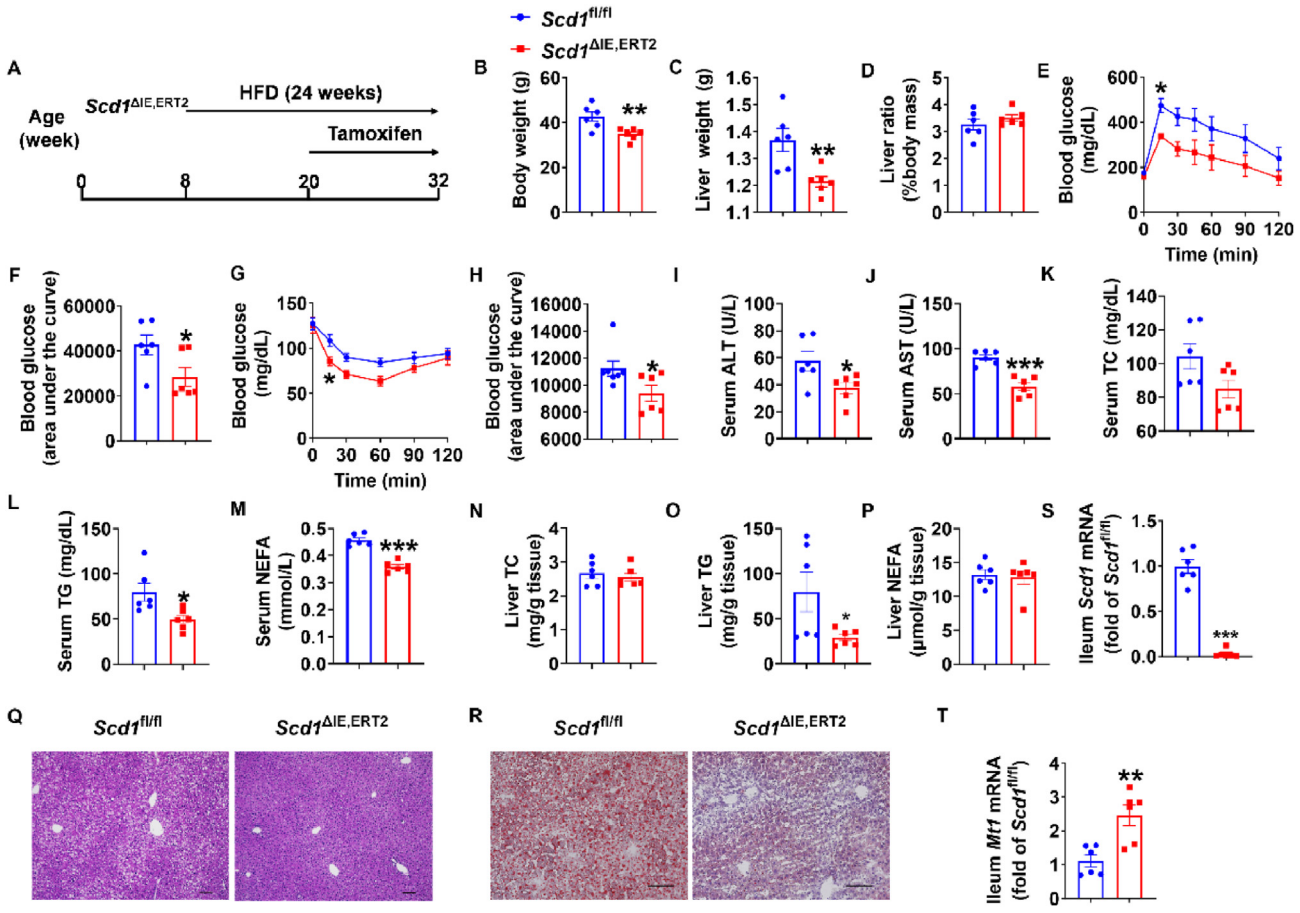

Figure 8 Intestine-specific inducible *Scd1* disruption ameliorated high-fat diet (HFD)-induced obesity and hepatic steatosis. *Scd1*$^{fl/fl}$ and *Scd1*$^{\Delta IE,ERT2}$ mice were first fed a high-fat diet (HFD) for 12 weeks and then injected weekly with tamoxifen while maintained on a HFD for another 12 weeks. (A) Experimental scheme. (B) final body weights. (C) Liver weights. (D) Liver index. (E) Glucose tolerance test (GTT). (F) GTT area under the curve. (G) Insulin tolerance test (ITT). (H) ITT area under the curve. (I) Serum alanine aminotransferase (ALT). (J) Serum aspartate aminotransferase (AST). (K) Serum total cholesterol (TC). (L) Serum triglyceride (TG). (M) Serum non-esterified fatty acid (NEFA). (N) Hepatic TC. (O) Hepatic TG. (P) Hepatic NEFA. $n = 6$. (Q, R) Representative hematoxylin and eosin staining (Q) and oil red O staining (R) of liver sections ($n = 3$ mice per group, three images per mouse per staining). Scale bar, 100 μm. (S, T) *Scd1*(S) and *Mt1* (T) mRNA in the ileum of *Scd1*$^{fl/fl}$ and *Scd1*$^{\Delta IE,\ ERT2}$ mice ($n = 6$). All data are presented as the mean ± SEM of biologically independent samples, analyzed using one-way ANOVA followed by Tukey's multiple comparisons test, except that for E and G, two-way ANOVA followed by Tukey's multiple comparisons test was used. $^*P < 0.05$, $^{**}P < 0.01$, $^{***}P < 0.001$, *Scd1*$^{\Delta IE,ERT2}$ *versus* *Scd1*$^{fl/fl}$.

mice were generated by crossing the *Scd1*$^{fl/fl}$ with the Villin-ERT2-cre mice to achieve temporal, intestine-specific *Scd1* disruption in the presence of tamoxifen. Decreased *Scd1* mRNA levels were found in the intestines of *Scd1*$^{\Delta IE,ERT2}$ mice compared to *Scd1*$^{fl/fl}$ mice after tamoxifen treatment (Fig. 8S). *Scd1*$^{\Delta IE,ERT2}$ mice were subjected to HFD feeding for 12 weeks to establish obesity and then treated with tamoxifen to activate the Cre recombinase while being maintained on HFD for another 12 weeks (Fig. 8A). *Scd1*$^{\Delta IE,ERT2}$ mice showed lower body weights and liver weights, and improved glucose tolerance and insulin sensitivity compared to *Scd1*$^{fl/fl}$ mice (Fig. 8B−H). Serum ALT and AST, hepatic and serum cholesterol levels, and hepatic triglyceride levels were markedly decreased in *Scd1*$^{\Delta IE,ERT2}$ mice, accompanied by increased expression of *Mt1* mRNA in the ileum of *Scd1*$^{\Delta IE}$ mice (Fig. 8I−P, Q, R, and T), suggesting that intestinal SCD1 deficiency could therapeutically ameliorate metabolic disorders in mice with established obesity.

4. Discussion

In the present study, intestine-specific disruption of *Scd1* in *Scd1*$^{\Delta IE}$ mice was found to protect against HFD-induced obesity, insulin resistance and hepatic steatosis. Mechanistically, deficiency of intestinal SCD1 results in increased MT1 levels, leading to decreased oxidative stress. Pharmacological inhibition of SCD1 by A939572 also exerts anti-obesity effects depending on the presence of intestinal, but not hepatic, SCD1, suggesting intestine SCD1 activity, but not hepatic SCD1, as a promising pharmacological target for the treatment of obesity and associated metabolic disease.

Previous work showed that global SCD1-deficient mice were protected from HFD-induced obesity due to increased energy expenditure[19]. While SCD1 protein is known to be highly expressed in both liver and adipose tissues, hepatocyte-specific

SCD1 knockout, adipocyte-specific SCD1 knockout, or both hepatocyte SCD1 and adipocyte SCD1 double-knockout mice failed to replicate the obesity-resistant effect of global SCD1 knockout mice during HFD feeding[21,23]. In line with these previous studies[21,23], there was no significant improvement in metabolic phenotypes in mice with liver-specific SCD1 deficiency during HFD feeding as revealed in the present study, indicating that SCD1 deficiency in an extrahepatic tissue is required to achieve the resistance to HFD-induced weight gain and hepatic steatosis. Interestingly, in the present study, while intestine is not the tissue with the highest expression of SCD1 among all organs, SCD1 is markedly induced upon HFD feeding in mice or obesity challenge in humans, and intestine-specific *Scd1* disruption recapitulated the obesity-resistant metabolic phenotype observed in global SCD1 deficiency in mice. The mechanism for this increase in SCD1 by a HFD is not known. In a previous publication, hepatic SCD1 activity index was reported to negatively correlate with liver fat in an obese human population but not in leaner participants[34], indicating that hepatic SCD1 activity may modulate liver fat content in humans. However, in the present study, no significant change of liver *SCD* mRNA level was found in overweight humans compared to normal controls, and hepatic SCD1 deficiency in mice failed to modulate both obesity and fatty liver. Hepatic SCD1 activity index is correlated with liver content only in obese individuals with a BMI>27 in the former study[34], and the difference between hepatic SCD1 activity index estimated from fatty acid pattern in serum very low density lipoprotein-TGs in the former study and hepatic SCD1 expression evaluated by mRNA levels in the present study may explain the discrepancy.

Given the key role of SCD1 in catalyzing the transformation of SFA to MUFA, the fatty acid profile, including the main SCD1 substrates (C16:0 and C18:0) and their corresponding products (C16:1 and C18:1), as well as other enriched fatty acids that could be generated from SCD1 enzyme products, was first examined in the intestine of HFD-fed $Scd1^{fl/fl}$ and $Scd1^{\Delta IE}$ mice in the present study. However, unexpectedly, no notable change in intestinal fatty acid levels was observed in $Scd1^{\Delta IE}$ mice compared to $Scd1^{fl/fl}$ mice. The intestine of HFD-fed mice is likely overwhelmed with HFD-enriched fatty acids, which could potentially mask the differences of any *de novo* fatty acid metabolites generated by intestinal SCD1. It was reported that enhanced inflammation and tumorigenesis was observed in mice with intestinal SCD1 deficiency only when an oleic acid-deficient diet was used but not when oleic acid-enriched chow diet was employed[22], which supported the view that dietary fatty acids could compensate for the absence of SCD1 activity in the intestine, thus masking the effects of loss or inhibition of SCD1. However, intestine tissue typically transports lipids instead of storing them. The intestine-derived lipids are usually packaged into triglyceride-rich lipoproteins that then enter the circulation where they are taken up by the liver and other tissues[35]. Indeed, decreased levels of unsaturated fatty acids were detected in the liver of HFD-fed $Scd1^{\Delta IE}$ mice. While the present study indicates that a intestinal SCD1 deficiency does not significantly change intestinal *de novo* lipogenesis and thus likely has a minor role in the observed phenotype, it is still not clear whether the reduced levels of unsaturated fatty acids in the livers of HFD-fed $Scd1^{\Delta IE}$ mice are a result or a causal factor in reducing obesity in HFD-fed $Scd1^{\Delta IE}$ mice.

A previous study in mice with skin-specific disruption of *Scd1*, and a more recent study using intestine-specific *Scd1* knockout mice demonstrated increased bile acid levels in the serum, which are responsible for antagonizing TGR5 in brown adipose tissue, contributing to the lean phenotype in conditional *Scd1*-null mice[31,32]. Additionally, a shift in bile acid composition towards more conjugated bile acids, especially taurine conjugated bile acids, was previously shown in mice with *Scd1* knockout in the skin or intestine[31,32]. In the present study, all tested bile acids, including primary and secondary bile acids, as well as unconjugated and conjugated bile acids, tended to decrease in the serum of 10-week HFD fed $Scd1^{\Delta IE}$ mice, with significantly lower levels in several secondary bile acids. However, no notable changes in gene expression related to bile acid synthesis and transport were found in the liver and no changes in bile acid reabsorption were noted in the intestine, suggesting no significant difference in enterohepatic circulation of bile acids between the two genotypes. The discrepancy between the previous reports and the present findings regarding bile acid changes in mice after loss of SCD1 in the intestine may be due to different background of mice, as well as different feeding regimens that were used. Furthermore, changes in the composition of the gut microbiota were found in the intestinal *Scd1* knockout mice, with several alterations in microbe species being associated with the change in plasma bile acids[32]. Thus, further investigation is needed to determine whether the differences in bile acid metabolites between the $Scd1^{fl/fl}$ and $Scd1^{\Delta IE}$ mice observed result from variations in gut bacteria and whether these changes in bile acids are responsible for the observed metabolic phenotypes.

Expression of the antioxidant gene *Mt1* was consistently found to be increased in the intestine of $Scd1^{\Delta IE}$ mice under chow, 4-week or 10-week HFD treatment compared to $Scd1^{fl/fl}$ mice. Thus the role of oxidative stress and MT1, other than the enzyme activity of SCD1, was suspected to contribute to the anti-obesity phenotype in $Scd1^{\Delta IE}$ mice. Previously, oxidative stress was reported to be positively correlated with obesity due to enhanced production of ROS from excess adiposity[12]. Oxidative stress is induced in circulation and tissues, including liver and intestine, in mice and rats by HFD feeding[36,37]. MT1, which belongs to the metallothionein family, was demonstrated to be a stress protein that prevents oxidative damage by quenching ROS through oxidation of Cys residues[33]. With increased expression level of *Mt1* mRNA detected in the intestine, decreased oxidative stress was observed in the intestine of $Scd1^{\Delta IE}$ mice under HFD treatment compared to the $Scd1^{fl/fl}$ mice. The increase in intestinal *Mt1* mRNA was observed in $Scd1^{\Delta IE}$ mice after short-term HFD feeding prior to the occurrence of the anti-obesity phenotype or even in chow-fed $Scd1^{\Delta IE}$ mice, indicating that enhanced MT1 expression along with improved oxidative stress could be a causal factor of the improved phenotype. Mice lacking both MT1 and MT2 were found to become obese after HFD feeding or long-term aging on chow diet with adipocyte enlargement and altered leptin signaling[38,39], while the inducer of MT1, zinc (Zn), was reported to be lower in the serum in obese individuals[40] and supplementation of Zn was found to decrease obesity in mice[41]. Since SCD1 protein possesses binding sites for Zn in its structure[42], the question arises whether the upregulated MT1 in mice with intestinal *Scd1* deficiency is due to increased Zn level that results from decreased Zn binding by SCD1. This issue warrants further investigation.

In the present study, intestinal SCD1 knockout reduced intestinal oxidative stress, thereby reducing systematic oxidative stress accompanied by induced MT1 expression both at the early and late stages of HFD feeding, while the anti-oxidant NAC feeding abolished the anti-obesity phenotype of intestine-specific *Scd1*-

null mice. These results may shed light on the underlying mechanism of the preventive role of MT1 against HFD-induced obesity in mice and suggest the importance of analyzing intestine-specific MT1 deficiency to fully understand the specific role of MT1 in metabolic disorders. Interestingly, with the current study revealing a novel role for the intestinal SCD1-MT1 signaling axis in modulating obesity progression at least partially by regulating intestine-derived oxidative stress, a previous study showed that the oxidative stress occurs more highly in the intestine compared to other tissues when sleep was deprived[43], the extent to which the small intestine among all organs, with its large surface area exposed to the challenge of excess nutrients prior to systemic absorption, contributes to obesity induction needs to be further explored. Accumulated ROS in white adipose tissues in obese mice was reported to result in dysregulation of adipocytokines, thus contributing to metabolic disorders[12], and oxidative stress was also shown to activate SREBP1C to increase lipogenesis[44]. In the present study, intestinal SCD1 deficiency was found to reduce intestinal oxidative stress, leading to a reduction of systematic oxidative stress as revealed by reduced levels of oxidative markers in the serum of *Scd1*$^{\Delta IE}$ mice. However, whether intestine restricts the oxidative stress to control obesity through decreasing oxidative stress in adipose tissue or liver and regulating adipocytokines or lipogenesis, warrants further studies.

Abnormal expression and activity of SCD1 was reported to be associated with an increased risk of various metabolic diseases[16,45-50], while the biggest challenge in SCD1 inhibitor development is the mechanism-based adverse effects such as dry skin and dry eye resulting from the systemic distribution of SCD1 inhibitors, thus limiting their effectiveness and therapeutic use[51]. Great efforts have been invested into the discovery of SCD1 inhibitors[52], especially approaches toward liver-targeted inhibitors accomplished using antisense oligonucleotides or utilizing liver-specific organic anion transporting polypeptides, which have been shown to reverse severe insulin resistance and hepatic steatosis while reducing mechanism-based toxicity in animal models[53,54]. However, it was noted that hepatic SCD1 deficiency actually fails to contribute to any obesity-associated metabolic disorders both in the present study and early publications[21,23], which is against the rational of current drug discovery strategy that targets hepatic SCD1 for treating metabolic disorders. More straightforward, A939572, a selective SCD1 inhibitor[55], was found to improve obesity dependent on intestinal SCD1 but not hepatic SCD1, in the present study. Whether the metabolically beneficial effect of SCD1 inhibition caused by other chemical SCD1 inhibitors is also dependent on intestinal SCD1 still requires further studies, the current study at least sheds light on the importance of intestinal SCD1 in maintaining metabolic homeostasis with A939572 as an exemplified chemical SCD1 inhibitor. These findings imply that intestine-restricted SCD1 inhibition could be another promising strategy to treat metabolic disorders, which helps minimize the adverse effects of systemic exposure. More importantly, the current study suggests that future drug discovery targeting SCD1 for treating metabolic disorders should consider the tissue-specific role of SCD1.

5. Conclusions

In conclusion, this study reveals a potential mechanism underlying the protective role of intestinal SCD1 in obesity associated with regulation of *Mt1* and oxidative stress. Genetic reduction or pharmacological inhibition of intestinal SCD1 protects mice from HFD-induced obesity, highlighting intestinal SCD1 as a potential target to treat metabolic disorders. These results may help guide the development of SCD1-targeting drugs for the treatment of obesity-associated metabolic disorders.

Acknowledgments

This study was supported by the National Cancer Institute Intramural Research Program, CCR, CIL, the Natural Science Foundation of Jiangsu Province (BK20241592, China) to Tingting Yan, National Natural Science Foundation of China (No. 82404732 to Tingting Yan, No. 81930109 and 82321005 to Haiping Hao, No. 82370848 and HY2022-7 to Lulu Sun, No. 62173005 to Zhipeng Zhang), the Project of State Key Laboratory of Natural Medicines, China Pharmaceutical University (SKLNMZZ202402 to Haiping Hao, China), and National Institutes of Health, National Institute of Diabetes and Digestive and Kidney Diseases (DK118093 to James N. Ntambi, USA). Yang Zhang was supported by the Eunice Kennedy Shriver National Institute of Child Health and Human Development (NICHD, USA). We thank the National Institute of Diabetes and Digestive and Kidney Diseases (NIDDK) Mouse Metabolism (National Cancer Institute, Bethesda, USA) for the mouse indirect calorimetry analysis.

Author contributions

Yangliu Xia: Writing − review & editing, Writing − original draft, Methodology, Investigation, Formal analysis, Data curation, Conceptualization. Yang Zhang: Investigation. Zhipeng Zhang: Investigation. Nana Yan: Investigation. Vorthon Sawaswong: Investigation. Lulu Sun: Supervision. Wanwan Guo: Investigation. Ping Wang: Investigation. Kristopher W. Krausz: Investigation. Oksana Gavrilova: Investigation. James N. Ntambi: Resources. Haiping Hao: Supervision. Tingting Yan: Writing − review & editing, Writing − original draft, Investigation, Conceptualization. Frank J. Gonzalez: Supervision.

Conflicts of interest

The authors declare that no conflict of interest exists.

Appendix A. Supporting information

Supporting information to this article can be found online at https://doi.org/10.1016/j.apsb.2024.11.022.

References

1. Bray GA, Kim KK, Wilding JPH. Obesity: a chronic relapsing progressive disease process. A position statement of the World Obesity Federation. *Obes Rev* 2017;**18**:715−23.
2. Papamargaritis D, le Roux CW, Holst JJ, Davies MJ. New therapies for obesity. *Cardiovasc Res* 2024;**119**:2825−42.
3. Haslam DW, James WP. Obesity. *Lancet* 2005;**366**:1197−209.
4. Friedman JM. The discovery and development of GLP-1 based drugs that have revolutionized the treatment of obesity. *Proc Natl Acad Sci U S A* 2024;**121**:e2415550121.
5. Nogueiras R, Nauck MA, Tschop MH. Gut hormone co-agonists for the treatment of obesity: from bench to bedside. *Nat Metab* 2023;**5**:933−44.
6. Ansari S, Khoo B, Tan T. Targeting the incretin system in obesity and type 2 diabetes mellitus. *Nat Rev Endocrinol* 2024;**20**:447−59.

7. Holst JJ. GLP-1 physiology in obesity and development of incretin-based drugs for chronic weight management. *Nat Metab* 2024;**6**:1866−85.
8. Lu J, Liu H, Zhou Q, Wang MW, Li Z. A potentially serious adverse effect of GLP-1 receptor agonists. *Acta Pharm Sin B* 2023;**13**:2291−3.
9. Patel C, Ghanim H, Ravishankar S, Sia CL, Viswanathan P, Mohanty P, et al. Prolonged reactive oxygen species generation and nuclear factor-kappaB activation after a high-fat, high-carbohydrate meal in the obese. *J Clin Endocrinol Metab* 2007;**92**:4476−9.
10. Chrysohoou C, Panagiotakos DB, Pitsavos C, Skoumas I, Papademetriou L, Economou M, et al. The implication of obesity on total antioxidant capacity in apparently healthy men and women: the ATTICA study. *Nutr Metab Cardiovasc Dis* 2007;**17**:590−7.
11. Vincent HK, Taylor AG. Biomarkers and potential mechanisms of obesity-induced oxidant stress in humans. *Int J Obes* 2006;**30**:400−18.
12. Furukawa S, Fujita T, Shimabukuro M, Iwaki M, Yamada Y, Nakajima Y, et al. Increased oxidative stress in obesity and its impact on metabolic syndrome. *J Clin Invest* 2004;**114**:1752−61.
13. Manna P, Jain SK. Obesity, oxidative stress, adipose tissue dysfunction, and the associated health risks: causes and therapeutic strategies. *Metab Syndr Relat Disord* 2015;**13**:423−44.
14. Talebi A, Dehairs J, Rambow F, Rogiers A, Nittner D, Derua R, et al. Sustained SREBP-1-dependent lipogenesis as a key mediator of resistance to BRAF-targeted therapy. *Nat Commun* 2018;**9**:2500−10.
15. Zou Y, Wang YN, Ma H, He ZH, Tang Y, Guo L, et al. SCD1 promotes lipid mobilization in subcutaneous white adipose tissue. *J Lipid Res* 2020;**61**:1589−604.
16. Hulver MW, Berggren JR, Carper MJ, Miyazaki M, Ntambi JM, Hoffman EP, et al. Elevated stearoyl-CoA desaturase-1 expression in skeletal muscle contributes to abnormal fatty acid partitioning in obese humans. *Cell Metab* 2005;**2**:251−61.
17. Dobrzyn P, Jazurek M, Dobrzyn A. Stearoyl-CoA desaturase and insulin signaling—what is the molecular switch?. *Biochim Biophys Acta* 2010;**1797**:1189−94.
18. Aljohani AM, Syed DN, Ntambi JM. Insights into stearoyl-CoA desaturase-1 regulation of systemic metabolism. *Trends Endocrin Met* 2017;**28**:831−42.
19. Ntambi JM, Miyazaki M, Stoehr JP, Lan H, Kendziorski CM, Yandell BS, et al. Loss of stearoyl-CoA desaturase-1 function protects mice against adiposity. *Proc Natl Acad Sci U S A* 2002;**99**:11482−6.
20. Sampath H, Flowers MT, Liu X, Paton CM, Sullivan R, Chu K, et al. Skin-specific deletion of stearoyl-CoA desaturase-1 alters skin lipid composition and protects mice from high fat diet-induced obesity. *J Biol Chem* 2009;**284**:19961−73.
21. Miyazaki M, Flowers MT, Sampath H, Chu K, Otzelberger C, Liu X, et al. Hepatic stearoyl-CoA desaturase-1 deficiency protects mice from carbohydrate-induced adiposity and hepatic steatosis. *Cell Metab* 2007;**6**:484−96.
22. Ducheix S, Peres C, Hardfeldt J, Frau C, Mocciaro G, Piccinin E, et al. Deletion of stearoyl-CoA desaturase-1 from the intestinal epithelium promotes inflammation and tumorigenesis, reversed by dietary oleate. *Gastroenterology* 2018;**155**:1524-38.e9.
23. Flowers MT, Ade L, Strable MS, Ntambi JM. Combined deletion of SCD1 from adipose tissue and liver does not protect mice from obesity. *J Lipid Res* 2012;**53**:1646−53.
24. Ratziu V, de Guevara L, Safadi R, Poordad F, Fuster F, Flores-Figueroa J, et al. Aramchol in patients with nonalcoholic steatohepatitis: a randomized, double-blind, placebo-controlled phase 2b trial. *Nat Med* 2021;**27**:1825−35.
25. Oballa RM, Belair L, Black WC, Bleasby K, Chan CC, Desroches C, et al. Development of a liver-targeted stearoyl-CoA desaturase (SCD) inhibitor (MK-8245) to establish a therapeutic window for the treatment of diabetes and dyslipidemia. *J Med Chem* 2011;**54**:5082−96.
26. Brocker CN, Yue J, Kim D, Qu A, Bonzo JA, Gonzalez FJ. Hepatocyte-specific PPARA expression exclusively promotes agonist-induced cell proliferation without influence from nonparenchymal cells. *Am J Physiol Gastrointest Liver Physiol* 2017;**312**:G283−99.
27. Yan T, Luo Y, Yan N, Hamada K, Zhao N, Xia Y, et al. Intestinal peroxisome proliferator-activated receptor alpha-fatty acid-binding protein 1 axis modulates nonalcoholic steatohepatitis. *Hepatology* 2023;**77**:239−55.
28. Whoe Consultation. Appropriate body-mass index for Asian populations and its implications for policy and intervention strategies. *Lancet* 2004;**363**:157−63.
29. Zhang Y, Yan T, Sun D, Xie C, Wang T, Liu X, et al. Rutaecarpine inhibits KEAP1−NRF2 interaction to activate NRF2 and ameliorate dextran sulfate sodium-induced colitis. *Free Radic Biol Med* 2020;**148**:33−41.
30. Luo Y, Yang S, Wu X, Takahashi S, Sun L, Cai J, et al. Intestinal MYC modulates obesity-related metabolic dysfunction. *Nat Metab* 2021;**3**:923−39.
31. Dumas SN, Ntambi JM. Increased hydrophilic plasma bile acids are correlated with protection from adiposity in skin-specific stearoyl-CoA desaturase-1 deficient mice. *PLoS One* 2018;**13**:e0199682.
32. Burchat N, Vidola J, Pfreundschuh S, Sharma P, Rizzolo D, Guo GL, et al. Intestinal stearoyl-CoA desaturase-1 regulates energy balance *via* alterations in bile acid homeostasis. *Cell Mol Gastroenterol Hepatol* 2024;**18**:101403.
33. Subramanian Vignesh K, Deepe GS Jr. Metallothioneins: emerging modulators in immunity and infection. *Int J Mol Sci* 2017;**18**:2197.
34. Stefan N, Peter A, Cegan A, Staiger H, Machann J, Schick F, et al. Low hepatic stearoyl-CoA desaturase 1 activity is associated with fatty liver and insulin resistance in obese humans. *Diabetologia* 2008;**51**:648−56.
35. Kozan DW, Derrick JT, Ludington WB, Farber SA. From worms to humans: understanding intestinal lipid metabolism *via* model organisms. *Biochim Biophys Acta Mol Cell Biol Lipids* 2023;**1868**:159290.
36. Cremonini E, Daveri E, Mastaloudis A, Adamo AM, Mills D, Kalanetra K, et al. Anthocyanins protect the gastrointestinal tract from high fat diet-induced alterations in redox signaling, barrier integrity and dysbiosis. *Redox Biol* 2019;**26**:101269.
37. Lasker S, Rahman MM, Parvez F, Zamila M, Miah P, Nahar K, et al. High-fat diet-induced metabolic syndrome and oxidative stress in obese rats are ameliorated by yogurt supplementation. *Sci Rep* 2019;**9**:20026.
38. Beattie JH, Wood AM, Newman AM, Bremner I, Choo KH, Michalska AE, et al. Obesity and hyperleptinemia in metallothionein (-I and -II) null mice. *Proc Natl Acad Sci U S A* 1998;**95**:358−63.
39. Sato M, Kawakami T, Kondoh M, Takiguchi M, Kadota Y, Himeno S, et al. Development of high-fat-diet-induced obesity in female metallothionein-null mice. *FASEB J* 2010;**24**:2375−84.
40. Abdollahi S, Toupchian O, Jayedi A, Meyre D, Tam V, Soltani S. Zinc supplementation and body weight: a systematic review and dose-response meta-analysis of randomized controlled trials. *Adv Nutr* 2020;**11**:398−411.
41. Chen MD, Liou SJ, Lin PY, Yang VC, Alexander PS, Lin WH. Effects of zinc supplementation on the plasma glucose level and insulin activity in genetically obese (*ob/ob*) mice. *Biol Trace Elem Res* 1998;**61**:303−11.
42. Shen JM, Wu G, Tsai AL, Zhou M. Structure and mechanism of a unique diiron center in mammalian stearoyl-CoA desaturase. *J Mol Biol* 2020;**432**:5152−61.
43. Vaccaro A, Dor YK, Nambara K, Pollina EA, Lin CD, Greenberg ME, et al. Sleep loss can cause death through accumulation of reactive oxygen species in the gut. *Cell* 2020;**181**:1307−28.
44. Sekiya M, Hiraishi A, Touyama M, Sakamoto K. Oxidative stress induced lipid accumulation *via* SREBP1c activation in HepG2 cells. *Biochem Biophys Res Commun* 2008;**375**:602−7.
45. Suppli MP, Rigbolt KTG, Veidal SS, Heeboll S, Eriksen PL, Demant M, et al. Hepatic transcriptome signatures in patients with varying degrees of nonalcoholic fatty liver disease compared with healthy normal-weight individuals. *Am J Physiol Gastrointest Liver Physiol* 2019;**316**:G462−72.
46. Piccinin E, Cariello M, Moschetta A. Lipid metabolism in colon cancer: role of liver X receptor (LXR) and stearoyl-CoA desaturase 1 (SCD1). *Mol Aspects Med* 2021;**78**:100933.
47. Yang B, Ding F, Wang FL, Yan J, Ye XW, Yu W, et al. Association of serum fatty acid and estimated desaturase activity with hypertension in middle-aged and elderly Chinese population. *Sci Rep* 2016;**6**:23446.

48. Mar-Heyming R, Miyazaki M, Weissglas-Volkov D, Kolaitis NA, Sadaat N, Plaisier C, et al. Association of stearoyl-CoA desaturase 1 activity with familial combined hyperlipidemia. *Arterioscler Thromb Vasc Biol* 2008;**28**:1193−9.
49. Ye Z, Zhuo Q, Hu Q, Xu X, Mengqi L, Zhang Z, et al. FBW7−NRA41−SCD1 axis synchronously regulates apoptosis and ferroptosis in pancreatic cancer cells. *Redox Biol* 2021;**38**:101807.
50. Huang Q, Wang Q, Li D, Wei X, Jia Y, Zhang Z, et al. Co-administration of 20(*S*)-protopanaxatriol (g-PPT) and EGFR-TKI overcomes EGFR-TKI resistance by decreasing SCD1 induced lipid accumulation in non-small cell lung cancer. *J Exp Clin Cancer Res* 2019;**38**:129.
51. Zhang Z, Dales NA, Winther MD. Opportunities and challenges in developing stearoyl-coenzyme A desaturase-1 inhibitors as novel therapeutics for human disease. *J Med Chem* 2014;**57**:5039−56.
52. Sun Q, Xing XR, Wang HY, Wan K, Fan RB, Liu C, et al. SCD1 is the critical signaling hub to mediate metabolic diseases: mechanism and the development of its inhibitors. *Biomed Pharmacother* 2024;**170**:115586.
53. Gutierrez-Juarez R, Pocai A, Mulas C, Ono H, Bhanot S, Monia BP, et al. Critical role of stearoyl-CoA desaturase-1 (SCD1) in the onset of diet-induced hepatic insulin resistance. *J Clin Invest* 2006;**116**:1686−95.
54. Kalliokoski A, Niemi M. Impact of OATP transporters on pharmacokinetics. *Br J Pharmacol* 2009;**158**:693−705.
55. von Roemeling CA, Marlow LA, Wei JJ, Cooper SJ, Caulfield TR, Wu K, et al. Stearoyl-CoA desaturase 1 is a novel molecular therapeutic target for clear cell renal cell carcinoma. *Clin Cancer Res* 2013;**19**:2368−80.